P2X purinergic receptors are required for correct cortical development in human brain organoids

Benito-León, M.; Serrano-López, J.; Llorente-Sáez, C.; Arribas-Blázquez, M.; Olivos-Oré, L.A.; Pravata, V.; ... ; Ortega, F.

Neuropharmacology 284 (2026) 110784

Contents lists available at ScienceDirect

Neuropharmacology

journal homepage: www.elsevier.com/locate/neuropharm

P2X purinergic receptors are required for correct cortical development in human brain organoids

María Benito-León [a,b,c,1], Julia Serrano-López [a,b,c,1], Celia Llorente-Sáez [a,b,c,d], Marina Arribas-Blázquez [b,d], Luis A. Olivos-Oré [b,c,d], Veronica Pravata [g,h], Raquel Pérez-Sen [a,b,c], Esmerilda G. Delicado [a,b,c], Micha Drukker [e,f], Antonio R. Artalejo [b,d], Silvia Cappello [g,h], Rosa Gómez-Villafuertes [a,b,c,*], Felipe Ortega [a,b,c,**]

[a] Departamento de Bioquímica y Biología Molecular, Universidad Complutense de Madrid (UCM), Madrid, Spain
[b] Instituto Universitario de Investigación en Neuroquímica (IUIN), Madrid, Spain
[c] Instituto de Investigación Sanitaria San Carlos (IdISSC), Madrid, Spain
[d] Departamento de Farmacología y Toxicología, Facultad de Veterinaria, Universidad Complutense de Madrid, Madrid, Spain
[e] Leiden University, 2333, CC, Leiden, the Netherlands
[f] Oncode Institute, 3521, AL, Utrecht, the Netherlands
[g] Division of Physiological Genomics, Biomedical Center (BMC), Faculty of Medicine, Ludwig-Maximilians-University (LMU), Munich, Germany
[h] Max Planck Institute of Psychiatry, Munich, Germany

ARTICLE INFO

Keywords:
Human cortical formation
Cerebral organoids
purinergic signaling
P2X receptors
Neural stem cells

ABSTRACT

The human neocortex represents a crucial evolutionary advance, the formation of which requires the tight and precise orchestration of both intracellular and extracellular signals. Structures grown in three-dimensional cultures, specifically human-induced pluripotent stem cells (hIPSCs)-derived cerebral organoids (COs), have been fundamental to study the signals that regulate the formation of the cortex, overcoming the limitations of 2D cultures. Amongst these, purinergic signaling driven by extracellular ATP and other nucleotides may encode crucial intercellular communications that govern central nervous system (CNS) development. The ATP that accumulates in the extracellular milieu can interact with both ionotropic P2X and metabotropic P2Y receptors on cells to exert its modulating effects. Although widely studied in different animal models, little is known about the expression and function of this signaling system in the human cortex. Thus, here we analyzed the expression of P2X receptor subunits comprehensively throughout the entire process of CO development, confirming that P2X receptors are functional in ventricular structures of the human cortex. Specifically, we detected the expression of P2X1, P2X4, and P2X6 in CO, showing distinct distributions in Nestin^{+} radial glial cells and/or DCX^{+} newborn neurons. Significantly, we also show how prolonged pharmacological inhibition of P2X activity affects CO development, resulting in smaller organoids with fewer and less well-organized cortical ventricles. Altogether, our findings point to a relevant role of purinergic signaling during the formation of the human cerebral cortex.

1. Introduction

The development of the human cerebral cortex is a complex and dynamic process driven by a precisely orchestrated series of genetic, environmental and biochemical factors. The generation of cortical neural cells depends on spatiotemporally coordinated events that control crucial processes like cell proliferation, cell fate determination, migration, maturation, synapse formation, network building, and finally, controlled apoptosis to model and prune the circuits established, hence ensuring the correct number of neurons are found at adequate locations. Alterations to any of these crucial processes may provoke severe central nervous system (CNS) abnormalities and malformations

This article is part of a special issue entitled: Tribute to Francesco Di Virgilio published in Neuropharmacology.

* Corresponding author. Departamento de Bioquímica y Biología Molecular, Universidad Complutense de Madrid (UCM), Madrid, Spain.
** Corresponding author. Departamento de Bioquímica y Biología Molecular, Universidad Complutense de Madrid (UCM), Madrid, Spain.
E-mail addresses: marosa@ucm.es (R. Gómez-Villafuertes), fortegao@ucm.es (F. Ortega).
[1] These authors contributed equally to this work.

https://doi.org/10.1016/j.neuropharm.2025.110784
Received 12 June 2025; Received in revised form 18 September 2025; Accepted 24 November 2025
Available online 28 November 2025

(Battal et al., 2015; Budday et al., 2015; Guerrini and Dobyns, 2014).

To comprehend the intricate paradigm of human cortical development it is crucial to gain a good understanding of the cell biology underlying the development of the main cell populations that form the cortex from neural stem cells (NSCs). However, to date most studies on NSCs have either being performed on animal models or on pure populations of particular human stem cell-derived cell types, rather than on the complete set of cell types that make-up the organ (Lancaster and Knoblich, 2014b). It should be noted that the organization of the human cortical progenitor domain is much more elaborated than the commonly used mouse models, therefore constituting a more complex scenario (Fietz et al., 2010; Hansen et al., 2010; Smart et al., 2002). Moreover, homogenous cultures derived from human stem cells lack the characteristic apical-basal polarity and they do not fully recapitulate the complex lineage of human NSCs *in vivo* (Conti and Cattaneo, 2010). Such limitations, implicit in previous studies, may be overcome by using three-dimensional cultures of developing tissues, called cerebral organoids (Lancaster and Knoblich, 2014b; Lancaster et al., 2013). Derived from human induced pluripotent stem cells (hIPSCs), COs contain more than one cell type, and better resemble the functional organization of human cortical structures, constituting the most accurate method currently available to study the development and cell biology of this crucial brain area. Specifically, COs have been shown to recapitulate key aspects of early brain development, including the generation of neural progenitors, layered neuronal populations, and developmental trajectories comparable to the human fetal cortex (Kanton et al., 2019; Lancaster et al., 2013; Velasco et al., 2019). Single-cell transcriptomic studies confirm a high degree of transcriptional similarity between organoid-derived cell types and fetal tissue, although some divergence appears at later maturation stages (He et al., 2024). Importantly, organoids can also establish signaling centers and express morphogens such as WNT, BMP, and SHH, thereby reproducing aspects of *in vivo* patterning (Renner et al., 2017; Xiang et al., 2017). Nonetheless, although slowly being addressed by new protocols, limitations exist in cerebral organoids, including variability across protocols, lack of vasculature, microglia, and relevant signaling that may diverge from *in vivo* profiles, particularly at later maturation stages (Bhaduri et al., 2020; Cakir et al., 2019; Park et al., 2023; Pellegrini et al., 2020; Zhang et al., 2023). Hence, COs provide us with an ideal tool to study the multiple mechanisms, both intracellular and extracellular, that govern human cortex formation of the regulatory signals thought to be involved in this cerebral cortex development, extracellular ATP and other nucleotides are considered to be among the most notable candidates (Zimmermann, 2006). In addition to the well-known intracellular functions of nucleotides, they also fulfil extracellular roles as they act as neurotransmitters/neuromodulators in the CNS. Purinergic signaling constitutes one of the oldest means of cell-to-cell communication, a complex system made-up of different transmitters, receptors, enzymes and transporters (Burnstock, 1972; Burnstock et al., 1970; Oliveira et al., 2016). The transmission of signals mediated by ATP begins with its loading into secretory vesicles, controlled by the vesicular nucleotide transporter (VNUT: (Bankston and Guidotti, 1996; Gualix et al., 1996; Gualix et al., 1999; Sawada et al., 2008). VNUT is expressed significantly in both the human and mouse CNS (Menendez-Mendez et al., 2017; Sawada et al., 2008), and it modulates various physiological and pathological processes (Menendez-Mendez et al., 2015; Paniagua-Herranz et al., 2020)reviewed in (Miras-Portugal et al., 2019). Once released into the extracellular space, ATP and other related nucleotides can interact with cell-surface purinoceptors (P2 receptors: (Burnstock et al., 2011), receptors that can be classified into two subfamilies: the ionotropic P2X and the metabotropic P2Y receptors (Burnstock, 2007b). P2X receptors are homo- or heterotrimers formed by the assembly of seven distinct subunits (P2X1-7), and they are ligand-gated ion channels that are permeable to Na^+, K^+ and Ca^{2+}. By contrast, there are eight distinct P2Y receptors in mammals, which are G-protein coupled receptors (GPCRs) activated by adenine and/or uridine nucleotides ($P2Y_{1,2,4,6,11,12,13,14}$) that mediate intracellular signaling through a variety of second messengers (Burnstock, 2007b; Burnstock et al., 2011). During embryonic development, both P2X and P2Y receptors induce transient calcium fluxes that are crucial for NSC differentiation, proliferation and fate determination (Glaser et al., 2013; Oliveira et al., 2016). If we focus specifically on cortical development, the $P2Y_1$ receptor is known to mediate calcium waves in radial glia, which helps to maintain their 'stemness' by preventing their premature differentiation (Weissman et al., 2004). In addition, P2X receptors are essential to establish functional neuronal networks in the murine cortex, also modulating the proliferation and death of neural progenitor cells (Fumagalli et al., 2017; Oliveira et al., 2016; Tang and Illes, 2017). As the CNS matures, purinergic signaling modulates glia-glia and neuron-glia interactions, mechanosensory transduction and autonomic functions (Abbracchio et al., 2009; Burnstock, 2007a). However, there is still a significant void in our understanding of the role of purinergic signaling during the formation of the human cortex.

Here, we initially focused on the ionotropic P2X receptors due to their crucial role in neuronal differentiation and neuroprotection, as well as their apparent implication in the progression of several neurodegenerative diseases (del Puerto et al., 2012; Diaz-Hernandez et al., 2012; Engel et al., 2012; Gomez-Villafuertes et al., 2009; Leon-Otegui et al., 2011; Miras-Portugal et al., 2015; Miras-Portugal et al., 2016; Ortega et al., 2009; Ortega et al., 2010). Accordingly, we carried out a comprehensive study of P2X subunit expression throughout CO formation, both at the transcriptional and translational levels, and assessing the main steps in CO development: hIPSCs, embryonic bodies (EBs), neuroepithelial induction and expansion, and finally, the development of the complete CO. We demonstrate the expression and activity of distinct ionotropic P2X channels within the cortical ventricles, the most reliable and reproducible cellular structures within the forebrain COs (Lancaster et al., 2013). Finally, we showed how the prolonged pharmacological inhibition of P2X signaling affects organoid development, resulting in smaller COs with fewer and less organized cortical ventricles and an enhanced neuronal maturation at early stages of development. Altogether, our findings extend the information previously obtained from murine models regarding the role of purinergic signaling in cortical embryonic development, highlighting the relevance of P2X ionotropic receptor expression and pointing to an important role for purinergic signaling during the formation of the human cerebral cortex.

2. Results

2.1. The expression of P2X ionotropic receptors during the formation of human forebrain organoids

To obtain a comprehensive picture of the expression of the different inotropic P2X family members during the formation of COs, we initially performed RT-qPCR experiments to analyze their transcripts and the variations in P2X expression as the neural human tissue is generated. As such, mRNA was isolated from the most relevant stages in CO formation (Lancaster and Knoblich, 2014a) and the data obtained by PCR were normalized to that of GAPDH (glyceraldehyde-3-phosphate dehydrogenase) house-keeping gene. The expression of the seven P2X subunits could be detected during at least one of the stages of CO formation analyzed: hIPSCs growing in culture; EBs 24h after their plating, EBs transferred to neural induction medium (6 days: NE); EBs with an expanded neuroepithelium (12 days: ExpNeu); and fully formed COs 37 days after transfer to Matrigel (Fig. 1). Accordingly, mRNA encoding the P2X1, P2X2, P2X3 and P2X4 subunits was detected at different levels at all the stages analyzed, except for P2X2 that was absent from the fully formed COs. The P2X4 subunit was that expressed most stably during organoid formation, from the initial stages to fully formed COs, when achieves the strongest expression (Fig. 1B–E). Furthermore, the P2X5 subunit was expressed most strongly in hIPSCs, subsequently diminishing until it was no longer detected in fully formed COs (Fig. 1F).

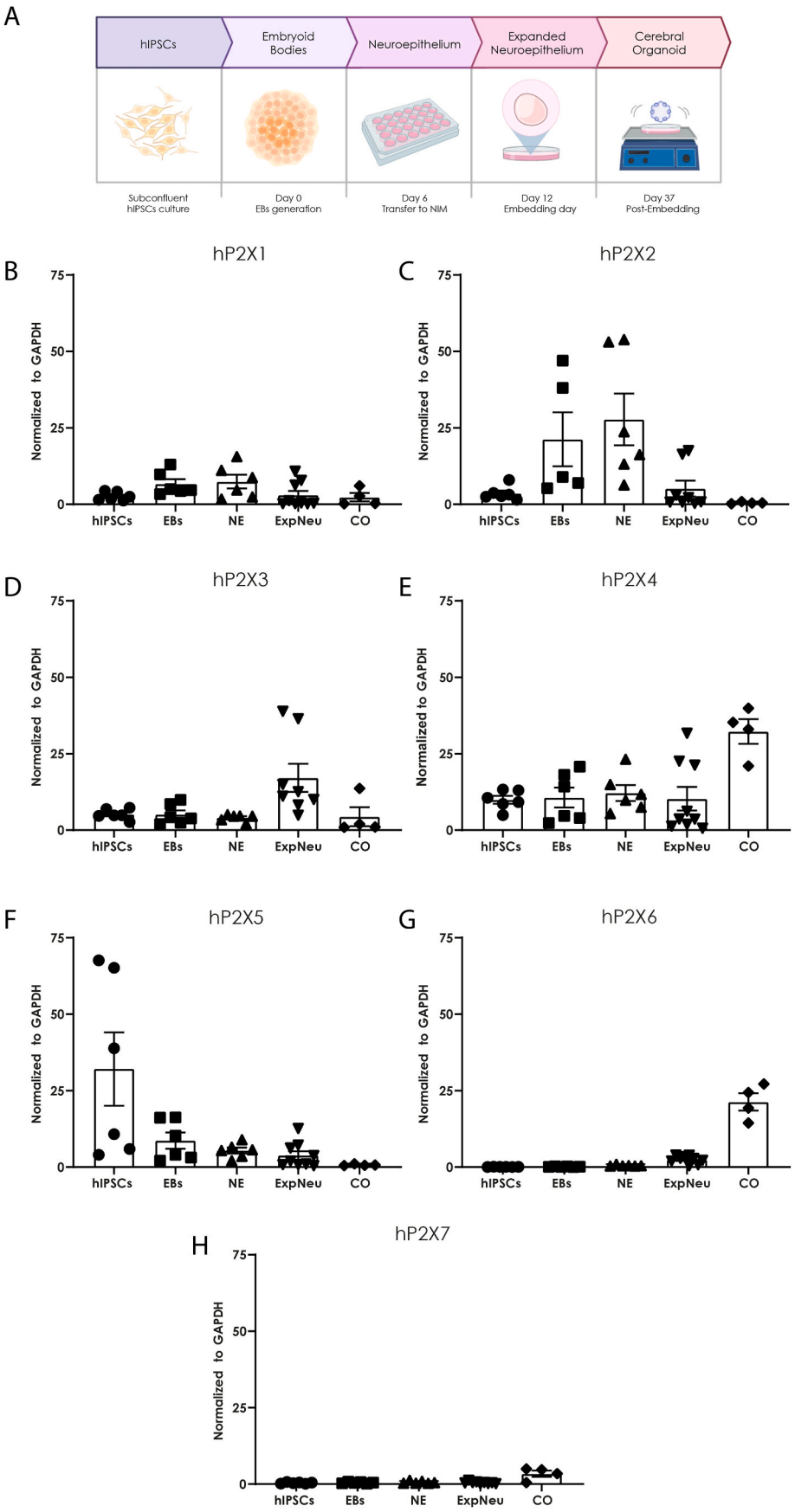

(caption on next page)

Fig. 1. Analysis of P2X subunit mRNA expression during the formation of human cerebral organoids. **A.** Scheme depicting the different stages of cerebral organoid (CO) development analyzed: hIPSCs, Embryonic bodies (EBs), Neuroepithelium (Ne), Expanded Neuroepithelium (ExpNeu) and fully developed organoids (COs). **B-H.** Expression of the P2X1 (B), P2X2 (C), P2X3 (D), P2X4 (E), P2X5 (F), P2X6 (G) and P2X7 (H) subunit mRNA normalized to GADPH expression across the different stages of CO formation. All graphs show the mean ± SEM of 6–9 EBs or COs performed in triplicate.

Finally, the expression of P2X6 and P2X7 subunits was barely detected in the initial stages studied, only reaching detectable levels in the fully formed COs (Fig. 1G–H).

This data was compared with that obtained from single-cell RNA sequencing experiments (scRNAseq) on 0 (hIPSCs) to 4-month-old human COs (Kanton et al., 2019), supporting the specificity of our results and adding information regarding the potential expression of the P2X receptors within specific cell populations. This database clusters the different cell populations present during the development of COs over a pseudo-time scale (Fig. S1A), and the scRNAseq data was generally consistent with our RT-qPCR results. Thus, the P2X2 and P2X3 subunits were detected in pluripotent stem cells, followed by their expression in the neuroectoderm/neuroepithelium, as well as in early neural precursors and radial glia. Moreover, the P2X4 subunit was the most strongly expressed at all stages, and in particular by neural precursors/radial glia cells and intermediate progenitors. By contrast, the P2X5 subunit was expressed most strongly by pluripotent stem cells, subsequently diminishing, while P2X6 and P2X7 were most prominent in early neural precursors and radial glia cells, having been almost totally absent at earlier stages of CO formation. Finally, the P2X1 subunit was expressed quite weakly, and it was restricted to pluripotent stem cells, radial glia cells and intermediate progenitors, unlike our previous experiments where this subunit was also expressed at intermediate stages (Fig. S1B). Finally, it is worth noting that although several subunits were expressed by different subtypes of differentiated neurons, we were unable to compare these results with our RT-qPCR experiments as our COs were harvested 37 days after embedding into Matrigel and, therefore, these cell populations were not yet generated (Kanton et al., 2019; Lancaster & Knoblich, 2014a, 2014b; Lancaster et al., 2013).

To confirm whether the P2X receptors were also translated into protein, the COs were analyzed in Western blots probed with antibodies raised against these subunits. Consequently, only the P2X1, P2X2, P2X3 and P2X4 receptors were detected in Western blots of COs at the initial stages (hIPSCs, EB, NE and ExpNeu), with P2X3 only present at the NE stage (Fig. 2A and B). Moreover, only the P2X1, P2X4 and P2X6 receptors were present in fully formed COs. Consistent with their mRNA expression, P2X4 was expressed most strongly in the fully formed COs with P2X6 being absent until the late stages of CO formation (Fig. 2C and D).

COs are heterogeneous structures that reliably reproduce the developing cortex, although they may also harbor retinal, hippocampal or choroid plexus tissues, amongst others (Lancaster and Knoblich, 2014a). Thus, to determine if the P2X receptors detected were indeed expressed in the developing human cortical structures, the expression of P2X1, P2X4 and P2X6 receptors in the cortical ventricles was assessed by

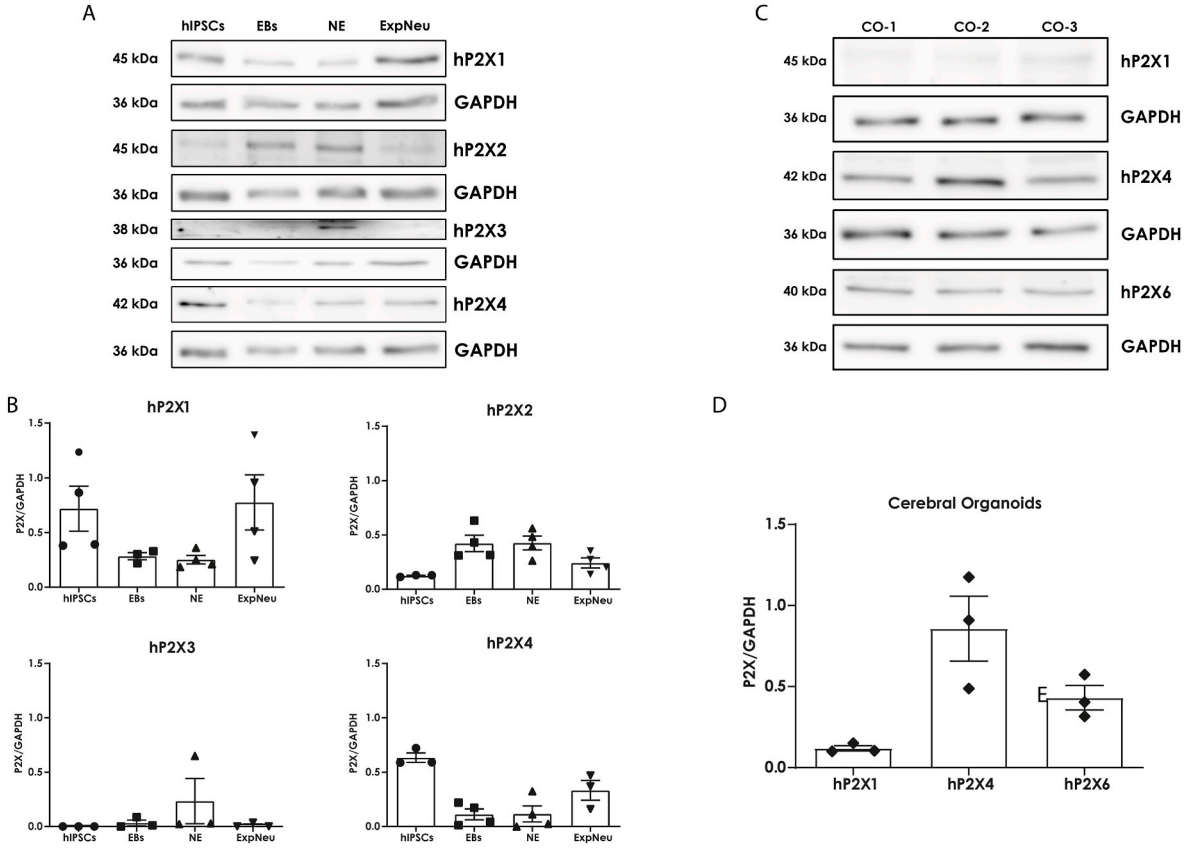

Fig. 2. Analysis of the P2X subunit protein during the formation of human cerebral organoids. The P2X receptor subunit protein was analyzed at the same time points described in Fig. 1. **A.** Western blots probed for the P2X receptors in hIPSCs, Embryonic bodies (EBs), Neuroepithelium (Ne) and Expanded Neuroepithelium (ExpNeu). **B**. Histograms depicting the expression of each receptor detected in A. **C.** Western blots probed for the P2X receptors detectable in fully developed organoids (COs). **D.** Histograms reflecting the expression of each receptor detected in C. All graphs show the mean ± SEM of 6–9 EBs or COs performed in triplicate.

immunohistofluorescence on cryosections of fixed 60-day-old COs derived from two different hIPSC lines, HMGU1 and 409B2 ((Cardenas et al., 2018; O'Neill et al., 2018; Okita et al., 2011). In addition, the potential association of these purinergic receptors with specific cell populations was evaluated using antibodies against Nestin (to label radial glia) and DCX (to label newborn neurons: (Kriegstein and Alvarez-Buylla, 2009; Noctor et al., 2002). Importantly, different patterns of P2X1, P2X4 and P2X6 receptor expression were detected in cortical ventricles, with P2X1 and P2X4 expressed significantly more in DCX newborn neurons than in Nestin positive cells but with no difference in P2X6 expression between these two populations (Fig. 3A and B) (see Table 1). These results were consistent with the analysis of both hIPSC lines, as the absence of significant differences between them further confirmed the validity of our results (Fig. 3C–E).

In sum, these experiments demonstrate that P2X receptors are expressed during the generation of human COs, confirming the presence of at least three members (P2X1, P2X4 and P2X6) in the developing cortical structures, co-localizing in both radial glia stem cells and newly generated cortical neurons.

2.2. P2X receptors are functional in developing cortical ventricles

Upon activation by ATP, their endogenous ligand, P2X receptors adopt an open configuration that facilitates Ca^{2+} and Na^{+} influx (Illes et al., 2021). Thus, calcium microfluorimetry and patch-clamp recordings were performed to assess whether the P2X receptors were fully functional in the formed ventricular structures. As 3D organoids are challenging models due to their structural heterogeneity and cell density, we took advantage of the 2D culture model of neural rosettes to perform these studies. Neural rosettes maintain apical-basal polarity and display the cytoarchitecture observed in the CO ventricles (Topol et al., 2015), thus representing a valuable tool for functional analysis.

Calcium microfluorimetry was performed in neural rosettes cultured for 14 days on glass coverslips, loaded with Fura-2 AM (a membrane-permeable synthetic calcium indicator) and superfused for 50 s with increasing concentrations of extracellular ATP. ATP-induced calcium transients were then assessed in several regions of interest within each rosette, so that cells at the center and periphery of the rosette could be analyzed (Fig. 4A–A'). Fura-2 ratio (F_{340}/F_{380}) traces on exposure to three different ATP concentrations (10 μM, 100 μM and 1 mM) reflected the calcium transients at the different regions of the rosettes (Fig. 4B). Fura-2 ratios, as an assay of cytosolic calcium concentrations, were significantly lower in response to 10 μM ATP (0.0158 ± 0.0011; n = 4) than to higher ATP concentrations (100 μM and 1 mM), suggesting that functional low- and high-affinity nucleotide receptors exist in both the central and peripheral cells of the rosette (Schmid and Evans, 2019). Maximal calcium transients were reached on exposure to 100 μM ATP (0.0296 ± 0.0019; n = 4), with 1 mM ATP eliciting a comparable calcium response (0.0283 ± 0.0030; n = 4: Fig. 4C).

Whole-cell patch clamp recordings were then obtained from 14-day-old cultured cells in the 2D brain organoids (Fig. 5A and B). The cells selected for recording had an ovoid or polygonal somata; the ovoid cells were situated outside the rosette (Type 1) or at its periphery (Type 2), these exhibiting bipolar processes unlike those at the center of the rosette (Type 4). Polygonal cells had multipolar cytoplasmic processes (Type 3) and were located in the periphery of the rosette.

Fast voltage-gated (+10 mV, 100 msec) inwardly-directed fast inactivating currents, probably due to Na^{+} ions entering the cell, were registered from Type 1 (100.1 ± 12.96 pA/pF, n = 15/15, 100 %), Type 2 (25.18 ± 7.96 pA/pF, n = 14/18, 78 %), Type 3 (11.10 ± 1.91 pA/pF, n = 8/12, 66 %) and Type 4 (12.99 pA/pF, n = 1/20, 5 %) cells (Fig. 5A–C). Inward currents were followed by sustained outward currents, most likely reflecting K^{+} efflux, in all Type 1 (54.17 ± 8.21 pC, n = 15), Type 2 (18.33 ± 2.45 pC, n = 18), Type 3 (10.99 ± 3.50 pC, n = 12), and Type 4 (15.11 ± 1.96 pC, n = 20) cells. It is worth noting that both inward current amplitude and outward current charge increased in a centrifugal manner, from Type 4 to Type 1 cells. Moreover, Type 1 and 2 cells with neuronal morphology exhibited action potential-like voltage changes upon injection of depolarizing current (Fig. 5A). These results suggest that cells in the 2D neural rosettes acquire electrical features resembling immature neurons, a neuronal profile that became apparent as cells leave the center of the rosette.

Next, we investigated the ability of 1 mM ATP (3 s) to gate membrane currents, as this concentration is sufficient to activate all P2X receptor types potentially found in the neural rosettes (Illes et al., 2021). Patch-clamp recordings revealed ATP-gated currents with decreasing amplitude from Type 1 (106.70 ± 44.63 pA/pF, n = 7/7; 100 %), to Type 2 (20.35 ± 4.86 pA/pF, n = 8/8; 100 %), Type 3 (4.22 ± 1.16 pA/pF, n = 7/8; 87.5 %) and Type 4 (2.30 ± 0.88 pA/pF, n = 11/17; 64.7 %) cells (Fig. 5D–G). Interestingly, P2X receptor-mediated currents showed different kinetics. So, the current showing an intermediate desensitization depicted in Fig. 5E, is reminiscent to that of recombinant P2X4 receptors (Schmid and Evans, 2019); likewise, the current shown in Fig. 5F, which was predominantly observed in Type 1 cells, may correspond to the activation of P2X1 or P2X3 receptors, which are known to mediate rapidly desensitizing currents (Egan et al., 2006; Schmid and Evans, 2019); last, the sustained current responses depicted in Fig. 5G are most consistent with the activation of P2X2, P2X6 and P2X7 receptors, which mediate minimally or non-desensitizing currents under sustained ATP exposure (Egan et al., 2006; Schmid and Evans, 2019).

2.3. Inhibiting P2X-dependent signaling alters normal development of cerebral organoids

Given that purinergic signaling is active within COs, we assessed whether P2X activity might influence the development of the cortical ventricular zone structures by exposing COs to a mixture of two non-selective P2 receptors antagonist (PPADS and BBG, 10 μM), to completely block the activity of any P2X receptor in the developing cortex (Illes et al., 2021). Antagonists were added to the cultures right after they were shifted to a neural induction medium and they were maintained throughout CO development (33 days). These antagonists were chosen as they are more stable and with a longer half-life than other agonists that are rapidly degraded by ectonucleotidases (Zimmermann, 2021).

Morphological changes in the COs were noticeable a few days after exposure to the antagonists. Specifically, by days 4, 6 and 8 (the latter coinciding with the embedding of the organoids into Matrigel), organoids were significantly smaller, less complex, and exhibited a higher cell density and fewer epithelial buds (Fig. 6A–C). These differences were consistent throughout CO development in the Matrigel until day 33 (Fig. 6A–C). Further analysis beyond this time point was not possible since the treated organoids tended to fuse within the culture (Fig. S2), making it difficult to measure the area of individual organoids. As indicated previously, COs are heterogeneous structures that may represent different areas of the human embryonic CNS (Lancaster and Knoblich, 2014a). Therefore, to analyze the specific effect of inhibiting P2X signaling on cortical ventricular structures, 60-day-old COs were stained with specific markers for the neural cell populations present in the developing cortex: Nestin and SOX2 for radial glia cells, TBR2 for intermediate progenitors, and DCX for newborn neurons (Villalba et al., 2021). In addition, the COs were stained for Ki67 as a read-out of active proliferation. Remarkably, organoids grown in the continued presence of PPADS and BBG had significantly fewer ventricles (0.2875 ± 0.2350, n = 4) relative to the controls (1.57 ± 0.07, n = 3), had a more disorganized cellular architecture, and were significantly smaller (182,341 ± 83,623 μm^2, n = 9) than the controls (368,609 ± 90,365 μm^2, n = 10; Fig. 7A–D). In terms of the specific neural cell populations, when P2X signaling was inhibited in the COs there were significantly fewer Nestin positive radial glia (1.14 ± 1.6 %Nestin area, n = 15) and TBR2 positive basal progenitors (0.72 ± 0.94, n = 13) than in the controls (Nestin

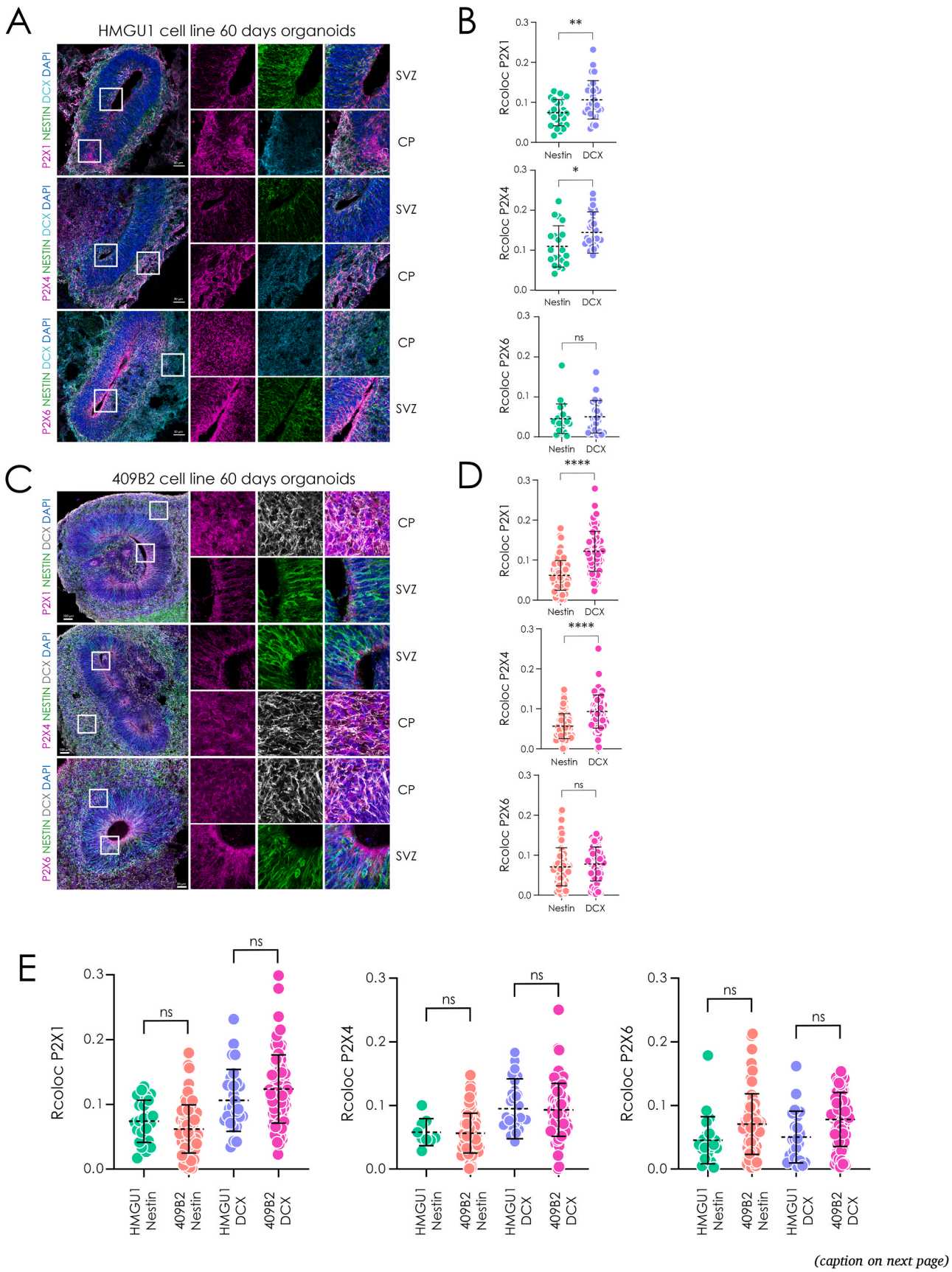

(caption on next page)

Fig. 3. Expression of the P2X receptors detected in cortical ventricle structures. A. Immunohistofluorescence of 60-day-old HMGU1-derived cortical organoid (CO) ventricles stained for P2X1, P2X4 and P2X6 receptors (magenta), Nestin (radial glia, green) and DCX (newborn neurons, white). **B.** Histogram depicting the quantification of Nestin^{+} and DCX $^{+}$ cells in which each P2X receptor is expressed (P2X1 **p = 0.0076, P2X4 *p = 0.0495, P2X6 p = 0.6638: unpaired T-test equal SDs assumed). **C.** Immunohistofluorescence of 60-day-old 409B2-derived CO ventricles stained for P2X1, P2X4 and P2X6 receptors (magenta), Nestin (radial glia, green) and DCX (newborn neurons, white). **D.** Histogram depicting the quantification of Nestin^{+} and DCX $^{+}$ cells that co-localize with each P2X receptor (P2X1 ****p = 0.0076, P2X4 ****p=<0.0001, P2X6 p = 0.3602: unpaired *t*-test). **E.** Relative quantification of both cell line-derived organoids (P2X1-Nestin p = 0.5694, P2X1-DCX p = 0.1153, P2X4-Nestin p = 0.8834, P2X4-DCX p = 0.2175, P2X6-Nestin p = 0.8834, P2X6-DCX p = 0.2176: unpaired T-test). The scale bars represent 50 μm in all images, except for the 409B2 cell line ventricles stained for P2X1 and P2X4 where they represent 100 μm. All graphs show the mean ± SD: *p < 0.05, **p < 0.01, ***p < 0.001, ****p < 0.000001.

Specific statistics:

Comparison	t	df	*p*-value	Significance
HMGU P2X1	2.783	50	0.0076	**
HMGU P2X4	2.304	46	0.0258	*
HMGU P2X6	1.112	43	0.2721	ns
409B2 P2X1	9.080	177	< 0.0001	****
409B2 P2X4	7.892	73	< 0.0001	****
409B2 P2X6	0.9183	132	0.3602	ns
Rcoloc Nestin-P2X1 HGMU vs 409B2	0.5706	110	0.5694	ns
Rcoloc DCX-P2X1 HGMU vs 409B2	1.586	120	0.1153	ns
Rcoloc Nestin-P2X4 HGMU vs 409B2	0.1471	82	0.8834	ns
Rcoloc DCX-P2X4 HGMU vs 409B2	1.242	88	0.2175	ns
Rcoloc Nestin-P2X6 HGMU vs 409B2	0.1471	82	0.8834	ns
Rcoloc DCX-P2X6 HGMU vs 409B2	1.242	88	0.2175	ns

(For interpretation of the references to color in this figure legend, the reader is referred to the Web version of this article.)

Table 1
The expression of the P2X1, P2X4 and P2X6 receptors in DCX and Nestin positive cells in each of the two lines (HMGU1 and 409B2).

Receptor	HMGU1 line		409B2 line	
	DCX	Nestin	DCX	Nestin
P2X1	0.11 ± 0.05 (n = 28)	0.07 ± 0.03 (n = 24)	0.12 ± 0.05 (n = 93)	0.06 ± 0.04 (n = 86)
P2X4	0.08 ± 0.07 (n = 12)	0.06 ± 0.02 (n = 9)	0.09 ± 0.04 (n = 78)	0.06 ± 0.03 (n = 75)
P2X6	0.05 ± 0.04 (n = 23)	0.05 ± 0.04 (n = 23)	0.08 ± 0.04 (n = 67)	0.07 ± 0.05 (n = 67)

positive 13.46 ± 7.20, n = 23; TBR2 positive 7.37 ± 5.39, n = 22; Fig. 7E–H). Finally, the presence of the antagonists also affected proliferation in the COs as there were significantly fewer KI67 positive area when P2X signaling was impaired (11.52 ± 8.26, n = 16) than in the controls (31.51 ± 11.81, n = 23; Fig. 7E–I).

Considering the overall decrease in organoid size and the reduction in the neural progenitor population, it is possible that cell cycle exit and neuronal differentiation are accelerated when P2X signaling is dampened, or alternatively, NPC death may increase. To discern between these two possibilities, we first assessed the number of caspase 3 positive apoptotic cells in cortical ventricles, which was apparently similar in the COs exposed to the antagonists (41.64 ± 10.73, n = 15) and in the control organoids (43.41 ± 12.12, n = 15; Fig. 7F–J). Thus, by conducting patch-clamp recordings from 2D-neural rosettes, we assessed whether neuronal differentiation was accelerated by inhibiting P2X signaling during development of these cortical structures. Fast inward current of 147 pA were recorded only in 1 of 8 Type 4 cells (12.5 %) from control COs, whereas all Type 4 cells (9/9, 100 %) assayed in COs exposed to the P2X antagonist, exhibited large amplitude inward currents (45.44 ± 16.25 pA/pF, p = 0.001). By contrast, no significant differences were evident in outward currents in cells from COs in which P2X signaling was impaired (22.41 ± 5.91 pC, n = 8) relative to those from control COs (15.13 ± 4.56 pC, n = 9; Fig. 8A and B). Remarkably, we observed that exposing 2D-cultures to the antagonists led to the formation of more neural rosettes at earlier time points (11 days in vitro; DIV), although they subsequently disappeared more rapidly than in the control conditions (14 DIV) (Fig. 8C). Together, these results confirm that exposure to the P2 non-selective antagonists (PPADS/BBG) accelerated neuronal differentiation as well as cortical structures growth, with most of the cells in the rosettes displaying an enhanced neuronal electrophysiological profile.

3. Discussion

This study presents evidence that the purinergic P2X receptors are expressed throughout the formation of human forebrain COs, which is particularly relevant given the lack of information regarding this important neurotransmitter system during human cortical embryonic development, as most studies performed to date have focused on animal models like zebrafish, mice or rats (Bestman et al., 2015; Guo et al., 2013). The data obtained reveal that purinergic P2X receptors are present from the initial stages of human cortical organoid development, consistent with a relevant role for this signaling system during CNS development as it appears to be one of the earliest systems of neural communication active during embryonic development in organisms (Zimmermann, 2006).

The P2X2 receptor has been seen to be expressed strongly by NPCs derived from murine embryonic stem cells (ESCs) and in rat NPC-derived neurospheres (Resende et al., 2008; Schwindt et al., 2011; Young et al., 2011). This is consistent with our results from COs in which the P2X2 receptor was detected when pluripotent stem cells appear, and its expression persisted quite intensely during the neuroepithelium development (EB-NE stages). Importantly, it is precisely at this NE stage when early NPCs arise (Lancaster and Knoblich, 2014a). The detection of P2X5 subunit expression was also interesting as it is one of the least studied receptors involved in purinergic signaling, with little information regarding its structure, pharmacology and function. These receptors were expressed most strongly in hIPSCs, subsequently diminishing and virtually disappearing in the fully formed COs. This is in line with evidence from mouse embryonic development where this receptor was detected immunohistochemically in neuroectoderm cells and in the cortical plate, disappearing progressively as cortical structures form (Guo et al., 2013). The P2X4 subunit was expressed most stably during

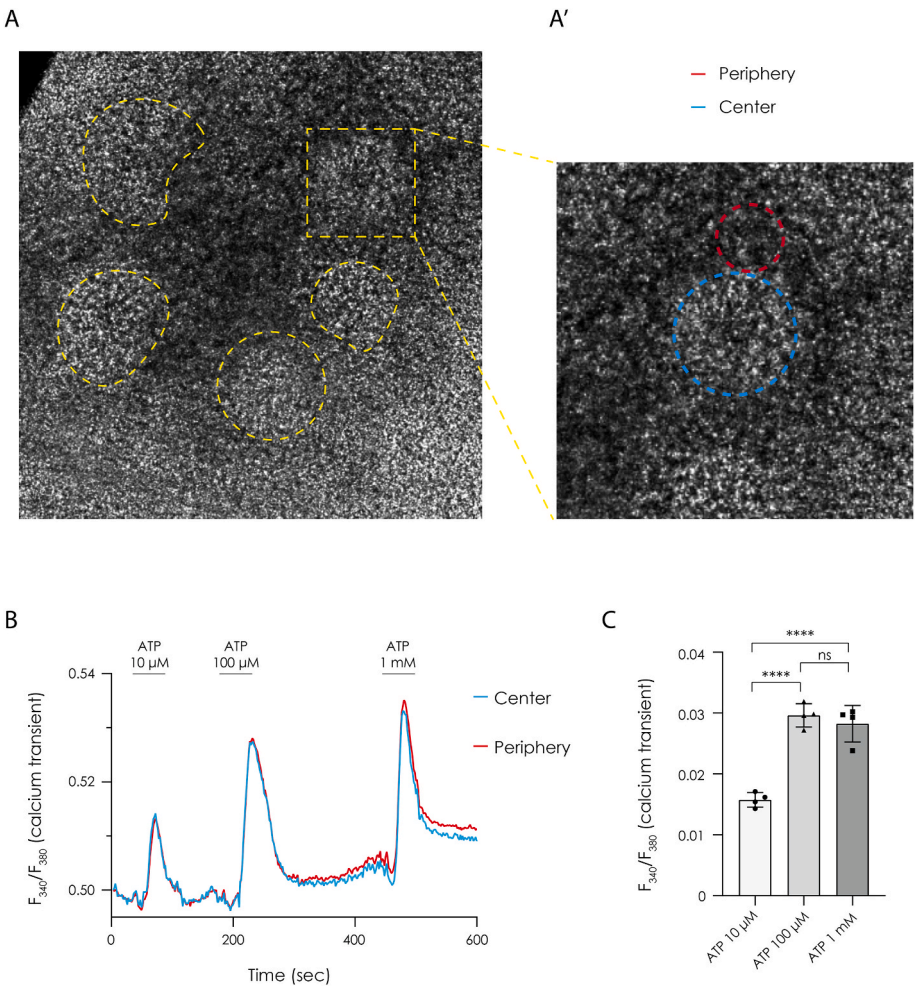

Fig. 4. ATP induces intracellular calcium transients in a 2D neural rosette culture model via purinergic receptor activation. A. Bright-field microscope image of a representative 2D brain organoid culture loaded with the calcium indicator Fura-2. The yellow circles outline several neural rosettes within the culture. One of these rosettes is magnified in panel **A′**, where the circles define selected regions of interest (ROIs) located in the center (blue circle) or at the periphery (red circle) of the rosette. **B.** Neural rosettes were superfused for 50 s with increasing concentrations of ATP, ranging from 10 μM to 1 mM, and the representative traces of intracellular calcium transients (expressed as the F_{340}/F_{380} ratio) induced by each ATP concentration indicated in the ROIs shown in panel A′ are displayed. **C.** The bar graph summarizes the peak amplitudes of the calcium transients elicited by the different ATP concentrations and expressed as the F_{340}/F_{380} ratio. Data are presented as mean ± SD (n = 4). Statistical analysis was performed using a one-way ANOVA, assuming a Gaussian distribution of residuals and equal standard deviations (validated by Brown-Forsythe and Bartlett's tests). Post hoc multiple comparisons were carried out using Sidak's test. The analysis revealed significant differences between ATP 10 μM (mean = 0.01575) and ATP 100 μM (mean = 0.02963), with a mean difference of −0.01388 ± 0.00153 (95 % CI: −0.01835 to −0.009402; $p < 0.0001$). Similarly, ATP 10 μM differed significantly from ATP 1 mM (mean = 0.02825), with a mean difference of −0.01250 ± 0.00153 (95 % CI: −0.01697 to −0.008027; $p < 0.0001$). No significant difference was observed between ATP 100 μM and ATP 1 mM, with a mean difference of 0.001375 ± 0.00153 (95 % CI: −0.003098 to 0.005848; $p = 0.7756$). (For interpretation of the references to color in this figure legend, the reader is referred to the Web version of this article.)

organoid formation, being the P2X receptor expressed most strongly within the COs. Moreover, it localized significantly in newborn neurons within the cortical ventricles, consistent with its presence in human ESCs, diminishing as they differentiate into NPCs to later increase again as new neurons are generated (Young et al., 2011). This pattern of expression may suggest that the P2X4 receptor is required during early neurogenic stages, as well as in the ensuing neuronal differentiation and maturation. Indeed, the closely related P2X7 receptor is required to maintain stem cell proliferation, modulating the behavior of both murine ventricular progenitors and their progeny (Glaser et al., 2014; Oliveira et al., 2016). Moreover, in mice, both the P2X4 and P2X7 receptors are involved in the correct differentiation, maturation and synapse formation of distinct neuronal populations (del Puerto et al., 2012; Diaz-Hernandez et al., 2012; Diaz-Hernandez et al., 2008; Gomez-Villafuertes et al., 2009; Young et al., 2011). Together with the P2X6 transcript, P2X7 mRNA was only found in fully formed COs, although this receptor was not detected as a protein. This is intriguing as this receptor is involved in controlling murine neurogenesis, neuronal differentiation and neuroprotection (Miras-Portugal et al., 2016; Miras-Portugal et al., 2017; Ortega et al., 2009, 2010; Ortega et al., 2011; Queipo et al., 2017). In addition, its deregulation is associated with several neurodegenerative diseases. Indeed, we previously indicated that these receptors are relevant during murine CNS formation, co-localizing widely with radial glia palisades within the circumventricular organs (Ortega et al., 2021). However, COs are heterogeneous structures that like cortical ventricular structures, may contain retinal, hippocampal, choroid plexus areas, amongst others (Lancaster and Knoblich, 2014a). Therefore, future studies aiming to analyze the specific expression of this receptor within cortical ventricular structures may be required to confirm whether it is present or absent during the formation of the human cortex.

Beyond the comprehensive analysis of the expression of these receptors during organoid formation, the purinergic signaling activity within the cortical ventricles was also studied. Sustained inhibition of

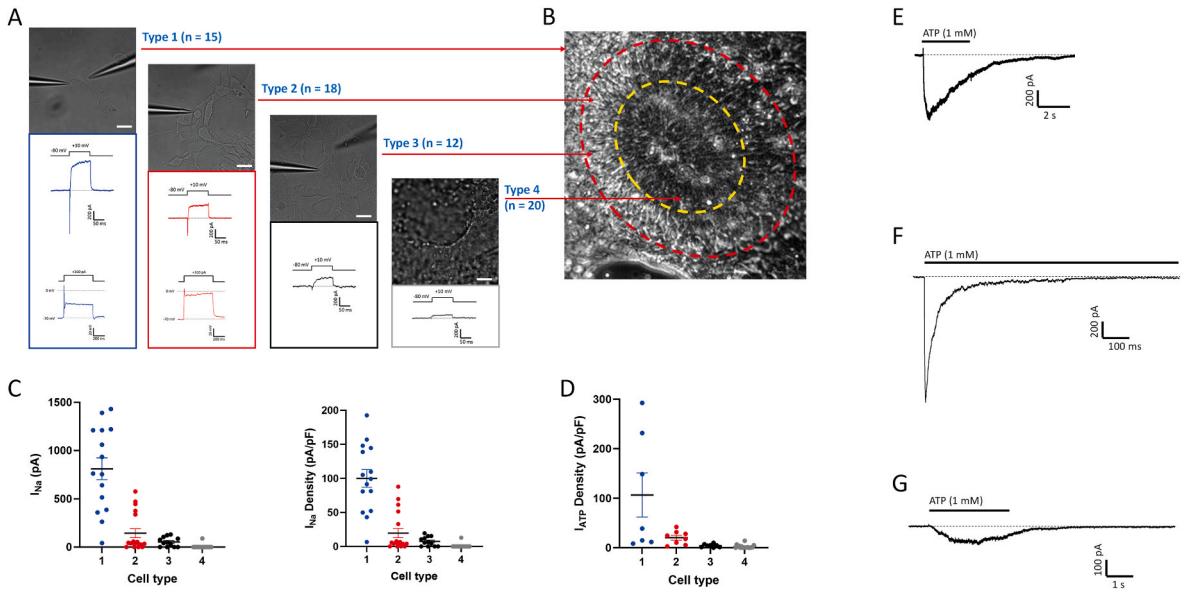

Fig. 5. Electrophysiological recordings from the 2D brain organoid culture system. A. . Upper panel: bright-field microscopy images of Type 1, Type 2, Type 3 and Type 4 cells (arranged left to right). A patch-clamp recording pipette placed on the somata of Type 1, Type 2 and Type 3 cells is shown, with a drug application pipette appearing close to Type 1 and 3 Typecells. Scale bar: 20 μm. Lower panels: voltage- and current-clamp recordings from imaged cells. Upper traces show inward and outward currents activated by a 100 msec voltage pulse to +10 mV from a V_h of −80 mV. The lower traces correspond to voltage changes elicited by a 160 pA current injection from a V_{comm} of −70 mV in Type 1 and 2 cells, depicting rapid initial voltage deflections akin to action potentials in immature neurons. **B.** Bright-field image of a rosette in a 2D brain organoid system in which the arrows indicate the cells shown in A. **C.** Left graph shows peak amplitudes of the inward currents, whereas the right graph depicts the total charge of the outward currents evoked by voltage depolarization in the four selected cell types. Statistical comparisons were performed using the Student's *t*-test for unpaired samples to evaluate differences in sodium currents between Type 1 cells and Type 2 ($P = 0.0001$; $DF = 31$), Type 3 ($P = 0.0001$; $DF = 25$) and Type 4 ($P = 0.0001$; $DF = 33$). Similarly, significant differences in potassium current charge were observed when comparing Type 1 cells to Type 2 ($P = 0.0001$; $DF = 31$), Type 3 ($P = 0.0002$; $DF = 25$) and Type 4 ($P = 0.0001$; $DF = 33$). **D.** Current density responses to ATP (1 mM; 3 s) are presented as mean ± SEM, based on the recorded cell Type indicated in panel A, and specifically 7 Type 1, 8 Type 2, 8 Type 3 and 17 Type 4 cells in D. Statistical analysis using the unpaired Student's *t*-test revealed significant differences in ATP-evoked responses when comparing Type 3 ($P = 0.0283$; $DF = 13$) and Type 4 ($P = 0.0011$; $DF = 22$) cells to the Type 1. **E-G.** Representative recordings of different profiles of ATP-induced currents obtained in the four cell types. Black lines above current traces indicate the duration of drug application.

P2X receptors by a combination of antagonists (PPADS and BBG) altered organoid development, reducing the number of ventricles and the population of radial glia cells and basal progenitors. It is worth noting that beyond the members of the P2X receptors, this combination of antagonists may also affect the metabotropic $P2Y_4$ and $P2Y_6$ receptors (Illes et al., 2021; von Kugelgen and Hoffmann, 2016) and thus, a contribution of these two receptors to the effects observed cannot be completely ruled out. Overall, the data obtained suggests that P2X signaling is involved in the lineage progression of cortical progenitors, its inhibition potentially inducing early cell-cycle exit and neuronal differentiation. In fact, the reduction in both radial glia and basal progenitors induced by P2X antagonism is consistent with the events in the later stages of cortical development, where radial glia numbers fall as the formation of the different cortical layers progresses (Kyrousi and Cappello, 2020; Molnar et al., 2019; Villalba et al., 2021). Indeed, fewer radial glia remains postnatally, although they appear to maintain the ventricular neurogenic niches in the CNS throughout the life of most mammals (Furutachi et al., 2015). However, the early exhaustion of this population observed upon inhibition of the P2X receptors, together with a clear disruption in the organization of the ventricular cortical structures studied may reflect a further decrease in neural progenitor self-renewal capacity. As such, the effects observed may be due to a dampened self-renewal capacity in combination with enforced early differentiation. Accelerated neuronal differentiation within the cortical structures was suggested by the patch-clamp recordings and the time-course studies of 2D-neural rosette formation in the presence or absence of the P2 non-selective antagonists (PPADS/BBG). This is consistent with our previous observations in neurogenic niches, such as the early postnatal cerebellum or the adult subependymal zone, environments in which modulating purinergic signaling through VNUT inhibition or $P2Y_{13}$ modulation induces self-renewal blockade and early neuronal differentiation, respectively (Lucía Paniagua-Herranz, 2024; Paniagua-Herranz et al., 2020). Moreover, evidence points to P2X signaling as a crucial step to maintain the proliferation of murine NPCs, promoting their differentiation when inhibited (Glaser et al., 2014; Oliveira et al., 2015). Modulation of P2X receptors also leads to hippocampal neuronal differentiation and synapsis formation (del Puerto et al., 2012; Diaz-Hernandez et al., 2008; Gomez-Villafuertes et al., 2009), further strengthening the concept of accelerated differentiation.

The data presented here also adds to the pre-existing knowledge as to how neurotransmitter activity regulates the behavior of NPCs (Berg et al., 2013; Giachino et al., 2014; Song et al., 2012; Tong et al., 2014; Trinchero et al., 2021; Xing and Huttner, 2020). Purinergic signaling stands out among other neurotransmission systems due to its early appearance. For example, glutamate receptors are detectable in the murine developing neocortex on embryonic day (E) 12 (Xing and Huttner, 2020), whereas purinergic receptors can already be detected on E9 (Cheung and Burnstock, 2002; Cheung et al., 2003; Ortega et al., 2021). In humans, the glutamatergic system is thought to regulate the proliferation capacity of NPCs isolated at 10–16 weeks of gestation (Suzuki et al., 2006). Conversely, the data presented here suggest that several P2X receptors would presumably be expressed and functional from the 5–6th week of gestation (Kyrousi and Cappello, 2020). This is consistent with our previous data from the postnatal cerebellum, where purinergic signaling, specifically VNUT, was effective before the onset of canonical neurotransmitter expression. Indeed, maximal VNUT expression correlated with the peak of post-natal neurogenesis, and it was present in the neurogenic niche before vesicular glutamate or GABA transporter expression was detected in the developing cerebellum (Paniagua-Herranz et al., 2020). Thus, our data suggests that NPCs may

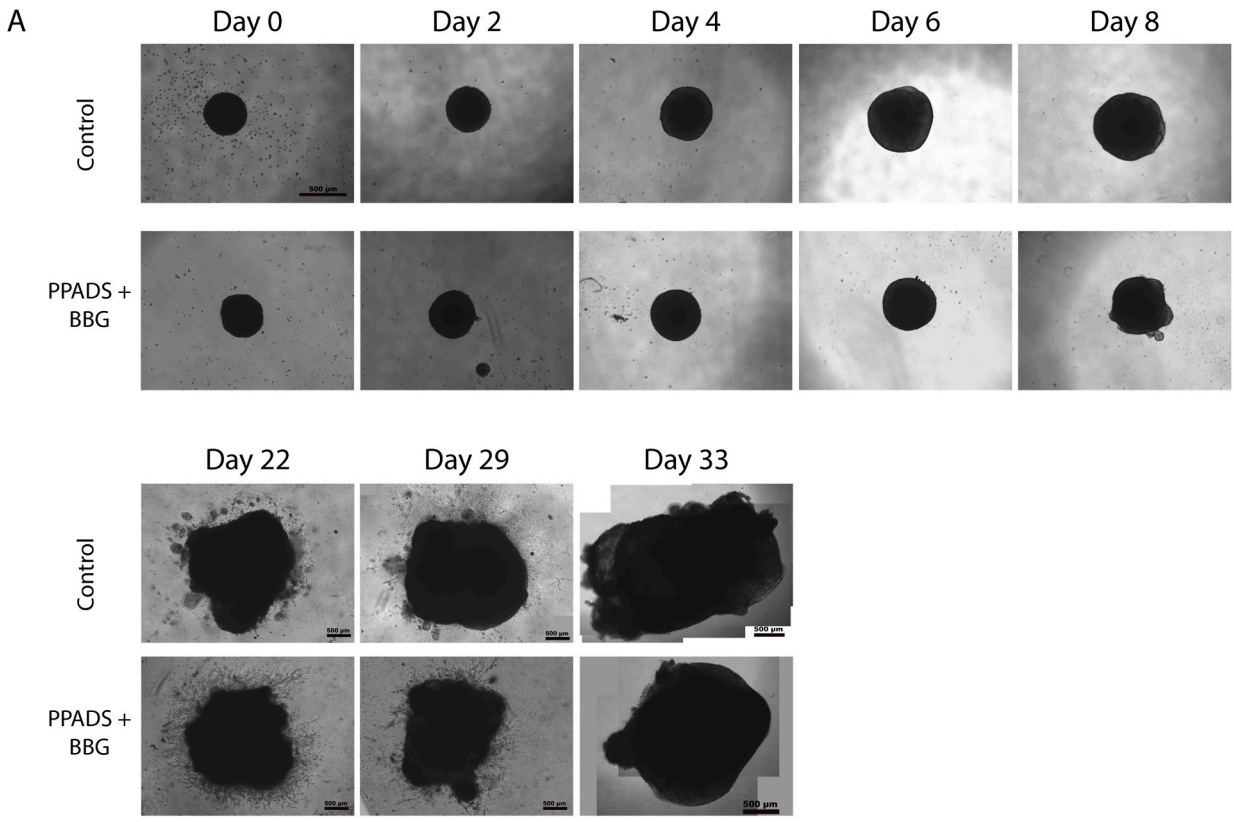

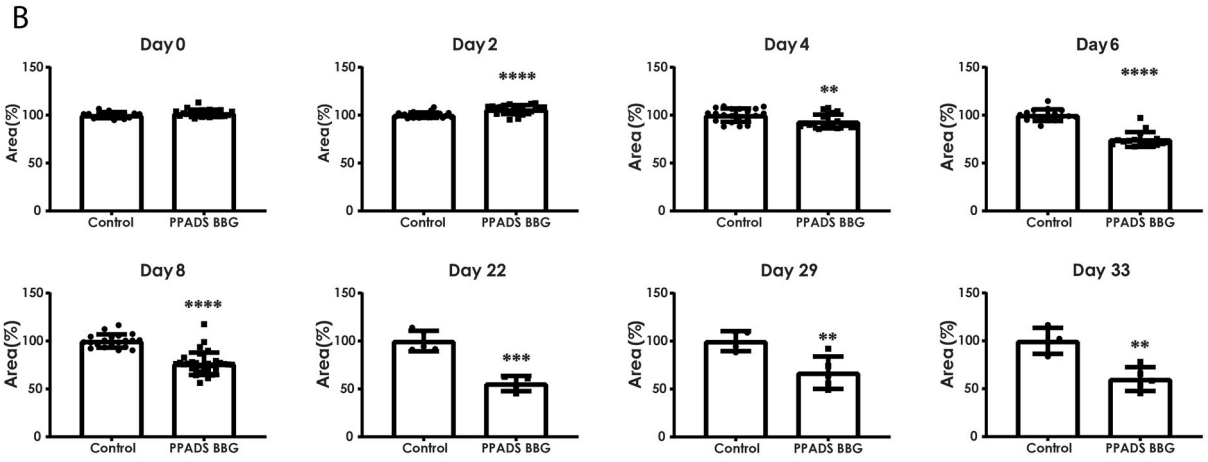

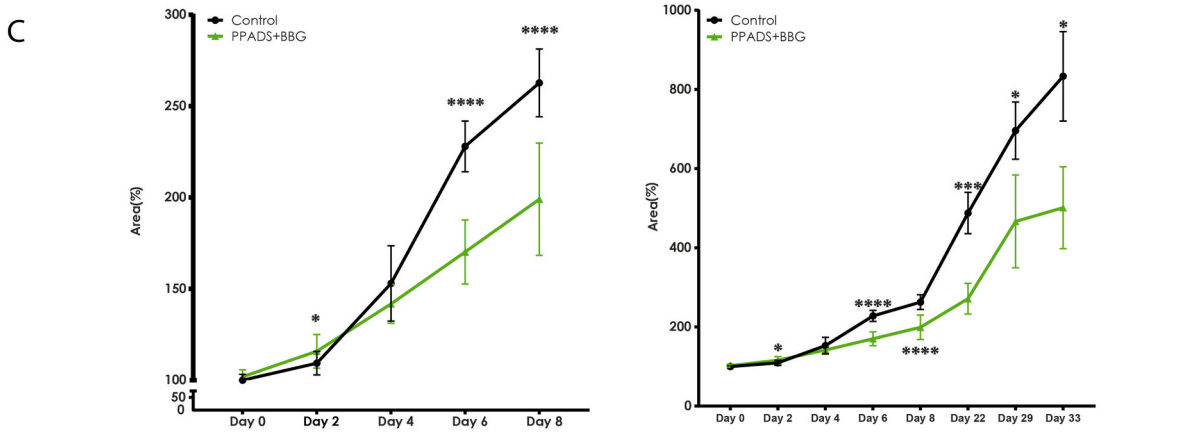

(caption on next page)

Fig. 6. The effect of sustained P2X inhibition with PPADS and BBG on the cell size in cerebral organoids. A. Bright-field images depicting the growth of control cerebral organoids (COs) or those maintained in the presence of PPADS/BBG. Scale bars represent 500 μM. **B.** Histogram depicting the comparison between the size of the control COs or those in the presence of PPADS/BBG. The areas are normalized to the control levels on each day (100 %). **C.** Graphs showing the evolution in size of the COs in culture, either under control conditions or following P2X receptor inhibition. All graphs represent the mean ± SD: *p < 0.05, **p < 0.01, ***p < 0.001, ****p < 0.000001 using an unpaired *t*-test with Welch's correction (B) or a multiple *t*-test with Holm-Sidak method (C).

Specific statistics:

B) Unpaired t test with Welch's correction. Df = Degrees of freedom.

Table Analyzed	Day 0	Day 2	Day 4	Day 6	Day 8	Day 22	Day 29	Day 33
P value	0,1051	<0,0001	0,0049	<0,0001	<0,0001	0,0002	0,0094	0,0035
P value summary	ns	****	**	****	****	***	**	**
Significantly different (P < 0.05)?	No	Yes	Yes	Yes	Yes	Yes	Yes	Yes
One- or two-tailed P value?	Two-tailed	Two-tailed	Two-tailed	Two-tailed	Two-tailed	Two-tailed	Two-tailed	Two-tailed
Welch-corrected t, df	t=1,664, df=35,13	t=5,171, df=36,34	t=2,991, df=37,94	t=10,33, df=28,48	t=9,191, df=49,95	t=7,134, df=6,988	t=3,602, df=6,693	t=4,543, df=6,260

C) Left (Days 0 to 8). Multiple t-Test. Statistical significance determined using the Holm-Sidak method, with alpha = 0.05.

Each row was analyzed individually, without assuming a consistent SD.

Number of t tests: 5.

	Significant?	P value	Mean of Control	Mean of PPADS+BBG	Difference	SE of difference	t ratio	df	Adjusted P Value
Day 0	No	0,114234	100	101,9	-1,913	1,182	1,619	36	0,114234
Day 2	Yes	0,008102	109,4	115,8	-6,483	2,337	2,774	44	0,024109
Day 4	No	0,037806	153	141,8	11,16	5,188	2,152	38	0,074184
Day 6	Yes	<0,000001	228	170,2	57,77	5,592	10,33	30	<0,000001
Day 8	Yes	<0,000001	262,7	199,1	63,67	7,63	8,344	50	<0,000001

C) Right (Complete Day 0 to 33). Multiple t-Test. Statistical significance determined using the Holm-Sidak method, with alpha = 0.05.

Each row was analyzed individually, without assuming a consistent SD.

Number of t tests: 8

	Significant?	P value	Mean of Control	Mean of PPADS+BBG	Difference	SE of difference	t ratio	df	Adjusted P Value
Day 0	No	0,114234	100	101,9	-1,913	1,182	1,619	36	0,114234
Day 2	Yes	0,008102	109,4	115,8	-6,483	2,337	2,774	44	0,032016
Day 4	No	0,037806	153	141,8	11,16	5,188	2,152	38	0,074184
Day 6	Yes	<0,000001	228	170,2	57,77	5,592	10,33	30	<0,000001
Day 8	Yes	<0,000001	262,7	199,1	63,67	7,63	8,344	50	<0,000001
Day 22	Yes	0,000236	487,7	271,3	216,4	31,46	6,878	7	0,001415
Day 29	Yes	0,011381	695,9	466,6	229,4	67,38	3,404	7	0,033756
Day 33	Yes	0,002501	833,1	501,2	331,9	72,23	4,594	7	0,012442

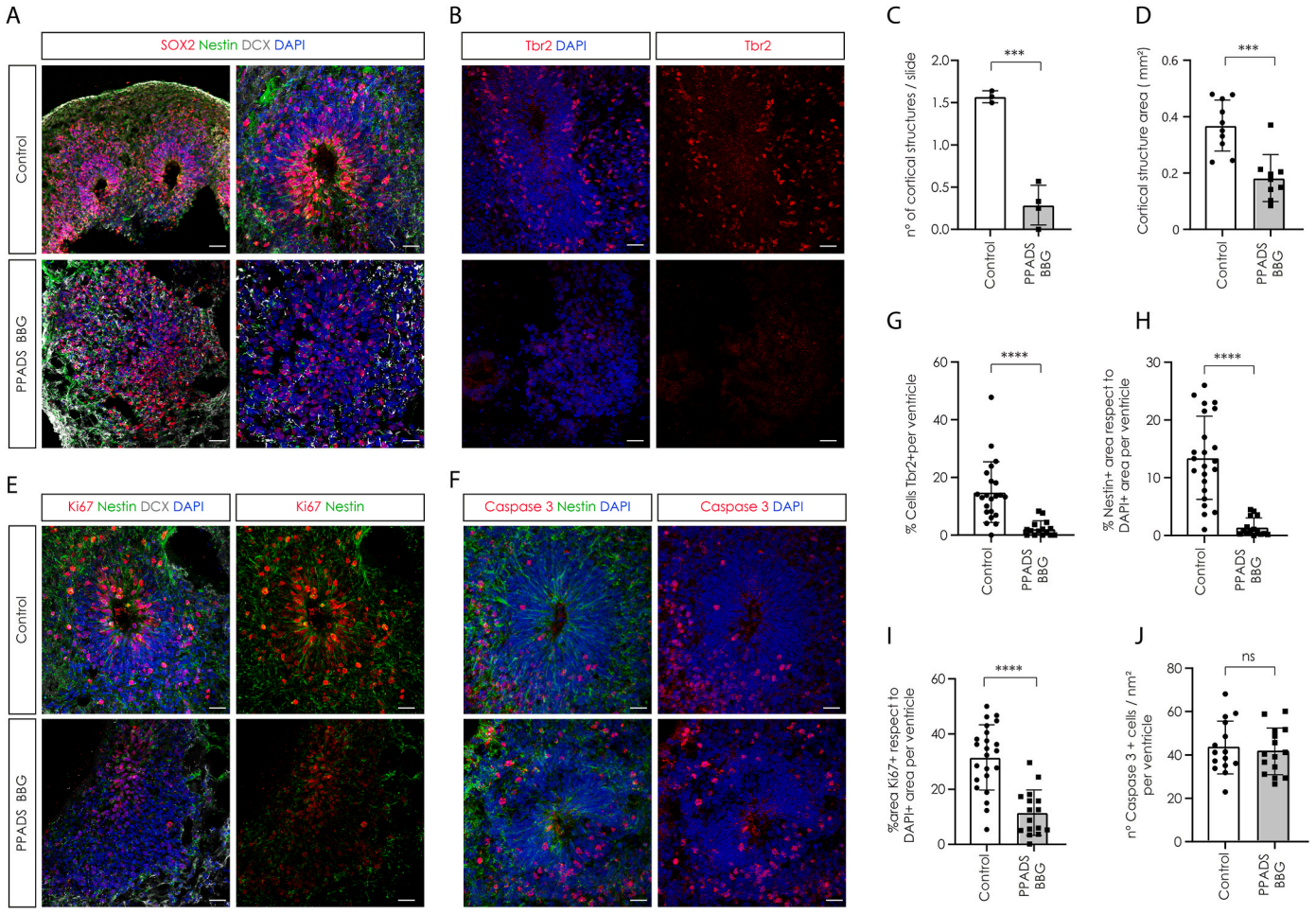

Fig. 7. The effect of sustained P2X inhibition with PPADS and BBG on the cortical ventricle structures within the cerebral organoids. A. Immunofluorescence staining of sections depicting the effect of PPADS/BBG on cortical ventricles as defined by the Nestin^{+} (green) and SOX2^{+} (red) neural progenitor area, and areas of new-born neurons (defined by DCX, white). Note the absence of an organized cortical structure in the presence of the inhibitors. **B.** Immunohistofluorescence showing the effect of sustained P2X inhibition on the population of Tbr2 positive cortical basal progenitors (red). **C.** and **D.** Histograms depicting (C) the number of cortical structures (***p = 0.003, unpaired T-test) and (D) the size of the control ventricles or when exposed to PPADS/BBG (***p = 0.0002, unpaired T-test). **E.** Immunohistofluorescence of sections showing the expression of the proliferative marker Ki67 (red) in the cortical ventricle areas co-stained with Nestin (green) and DCX (white). **F.** Confocal pictures reflect the expression of apoptotic cells in the ventricles stained for active Caspase-3 (red) and their relation to Nestin staining (green). All the sections were stained with DAPI to label the cell nuclei. **G-J.** Histogram depicting the quantification of the cell populations studied: (G) Tbr2^{+} basal progenitors (***p = 0.0001, unpaired T-test), (H) Nestin^{+} radial glia (****p=<0.0001, unpaired T-test), (I) Proliferative cells Ki67^{+} (****p=<0.0001, unpaired T-test), and (J) apoptotic cells labelled for Caspase 3 (ns, p = 0.6744, unpaired T-test). The scale bars represent 50 μm in the two left-most images and 25 μm in the remaining images. All graphs show the mean ± SD. *p < 0.05, **p < 0.01, ***p < 0.001, ****p < 0.000001.

Specific statistics:

Comparison	t	df	p-value	significance
nº of cortical structures/slide	8.963	5	0.0003	***
Cortical structure area	4.646	17	0.0002	***
% Cells Tbr2+ per ventricle	4.387	33	0.0001	***
% Nestin area r. DAPI per ventricle	6.335	36	<0.0001	****
% Area Ki67+ r. DAPI per ventricle	5.842	37	<0.0001	****
nº of Caspase-3 cells/nm² per ventricle	0.4245	28	0.6744	ns

(For interpretation of the references to color in this figure legend, the reader is referred to the Web version of this article.)

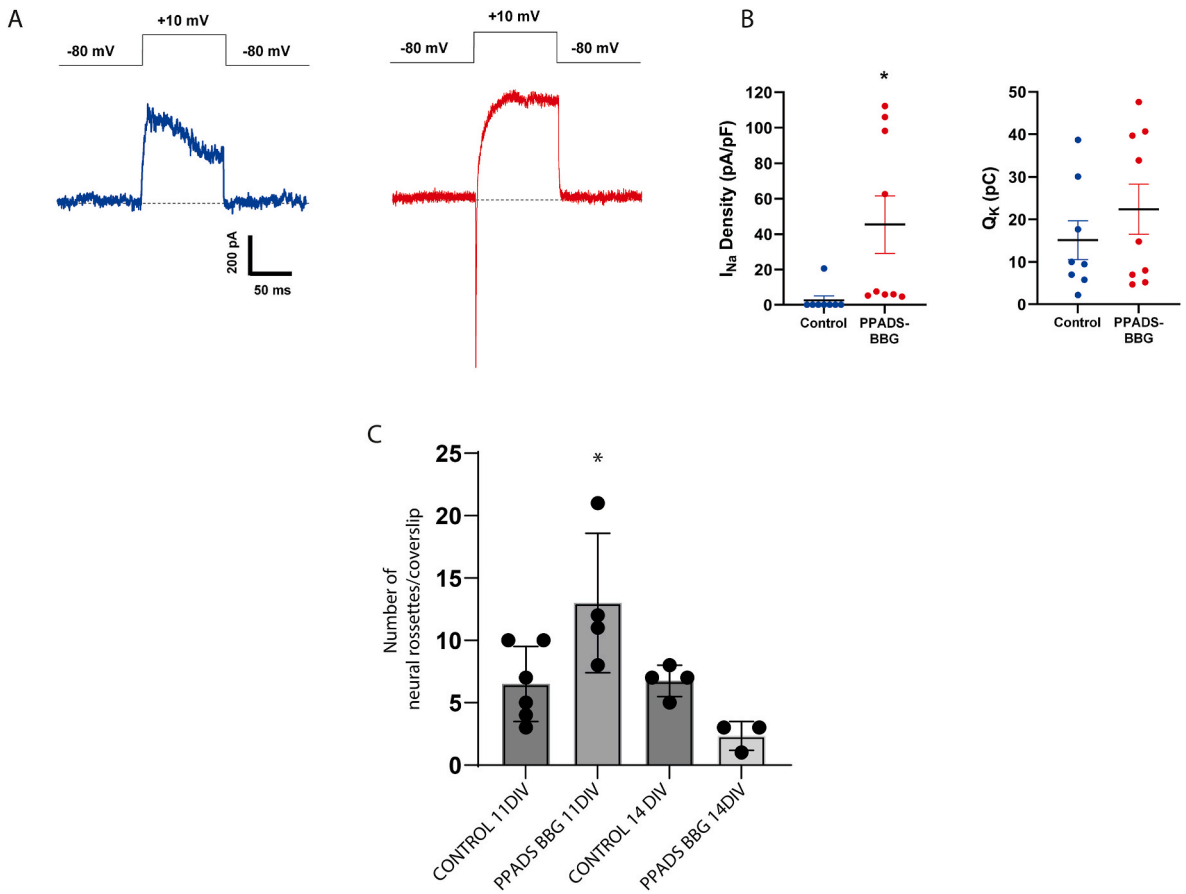

Fig. 8. Effect of BBG and PPADS on neuronal maturation of Type 4 cells. A. A. Voltage-clamp recordings obtained from control Type 4 cells (left) or exposed to BBG (10 μM) and PPADS (10 μM) (right). The voltage protocol is shown above the recordings (+10 mV for 100 msec from a V_h of −80 mV). **B.** Peak amplitudes of inward currents (left graph) and the charge of the outward currents (right graph) evoked by membrane depolarization in control cells (n = 8) and cells exposed to P2X antagonists (n = 9) from the experiments shown in A. Data are the mean ± SEM of the number of cells indicated. Statistical significance was assessed using the Student's *t*-test for unpaired samples (P = 0.0269; DF = 15). **C.** Bar graph of the number of neural rosettes after 11 and 14 days in vitro (DIV) in the absence and the presence of PPADS/BBG. Data represent the means ± SD: *p < 0.05 (One-way ANOVA).

use purinergic communication during development before other neurotransmitter systems are fully established. Consequently, the purinergic system may be postulated as a primary cell-to-cell communication network within neurogenic niches, enabling NPC lineage progression to be fine-tuned.

In summary, we employed here an organoid-based model to analyze comprehensively the expression of purinergic P2X receptors during human cortical development, pointing to a potential requirement for purinergic signaling in the correct development of ventricular cortical structures. Moreover, the data presented opens new avenues to study the individual contribution of each P2X receptor in the regulation of NPC behavior during this crucial developmental period, as well as a potential relationship between altered purinergic signaling and developmental malformations of the human cortex.

4. Materials and methods

4.1. Antibodies and chemicals

The antibodies used in this study were raised against: P2RX1 (APR-001), P2RX2 (APR-003), P2RX3 (APR-016), P2RX4 (APR-002), P2X6 (APR-013), P2RX7 (APR-004) P2X7 Blocking peptide Control (BLP-PR004), all for Alomone Labs; GAPDH (G9545) and Nestin (MAB5326), both from Sigma-Aldrich; SOX2 (AB5603) and doublecortin (DCX, AB2253), both from Millipore; Tbr2 (ab23345) from Abcam; and Ki67 (RM-9106-S) from Fisher Scientific. The secondary antibodies used were conjugated to: horseradish peroxidase (P0448 and P0260: Dako); Alexa Fluor® 488 or 555 (A10680 and A-21428: ThermoFisher Scientific), used in immunofluorescence analysis; Cy™5, anti-guinea pig (706-175-148: Jackson Immunoresearch); Biotin (65–6140) and Alexa Fluor® 546 Streptavidin (S11225: Invitrogen). The cell nuclei were counterstained with 4′,6-diamidino-2-phenylindole (DAPI, D1306: Fisher Scientific).

The Rock inhibitor Y-27632 (72302) and mTeSR1 medium (85850) were obtained from STEM Cell Technologies, and the SMAD inhibitors LDN193189 (6053) and SB431542 (1614) were purchased from Tocris. The basic fibroblast growth factor (bFGF 100-18B) was acquired from PreproTech, Matrigel® (35234) was from Corning and the cell-permeant Fura-2 acetoxymethyl ester calcium probe (Fura-2 AM, 11524766) was purchased from Molecular Probes. The 2-mercaptoethanol (8057400005) came from Merck and the Mycoplasma Gel Detection Kit (90.021–4542) was from Biotools. The Colagenase IV (17104019), laminin (23017-015), N2™ supplement (17502048), B27 supplement with vitamin A (17504044), B27 supplement without vitamin A (12587010), KnockOut™ serum replacement (KOSR, 10828010), hESC-quality fetal bovine serum (10270106), penicillin/streptomycin antibiotic solution (P/S 15070063), antimycotic amphotericin B (15290026) and Dispase® (17105041) were all obtained from ThermoFisher Scientific. Finally, paraformaldehyde (PFA), MEM non-essential amino acid solution (MEM-NEEA, M7145), heparin (H3149), insulin (I9278), Accutase® (A6964) and poly-L-ornithine (P3655) were acquired from Sigma-Aldrich.

4.2. Cell lines and pluripotent stem cell culture

All cell cultures, including neural rosette and organoid cultures, were performed with the hIPSC HMGU1 line (kindly provided by Dr. Micha Drukker, Institute of Stem Cell Research, Helmholtz Zentrum München, Germany). The HMGU1 line was originally derived from foreskin fibroblasts (male, newborn). Unguided brain organoids were derived from the HPS0076:409B2 cell line (Riken), which originated from dermal fibroblasts (female, 36 years old). Organoids were generated according to the protocol of Lancaster et al. (2013) at the Biomedical Center LMU (Germany) and used to confirm purinergic distribution among cortical structures. The hIPSCs were maintained at 37 °C in complete mTeSR1 medium on 6-well plates coated with Matrigel® under 5 % CO_2. All cell cultures were regularly tested for mycoplasma contamination.

4.3. Differentiation of neural rosettes

A previously reported method was followed to obtain neural rosette cultures (Topol et al., 2015). In brief, hIPSCs were grown and expanded in complete mTeSR1 medium until they were sub-confluent, and the cells were then detached from the plate as large colonies using collagenase IV (1 mg/ml) diluted in DMEM/F12. After gently washing the colonies twice with DMEM/F12, they were resuspended in 2 mL of N2/B27 medium (DMEM/F12, 1 % GlutaMAX, 1 % N2™ supplement, 1 % B27 without vitamin A) and then 1.3 mL of this suspension was transferred to each well of ultra-low attachment 24-well plates. Overnight, colonies formed floating spherical clusters named "embryoid bodies" (EBs) and on the second day, the medium was removed, the EBs were washed with DMEM/F12 and they were then fed with N2/B27 medium supplemented with two SMAD inhibitors: LDN193189 (0.1 μM) and SB431542 (10 μM). Neuralization occurred from days 3–7 in the context of dual SMAD inhibition, and the EBs were fed every second day with N2/B27 medium supplemented with the SMAD inhibitors. On day 7 the EBs were transferred to 24-well plates containing 12 mm glass coverslips coated with poly-L-ornithine (50 μg/mL) and laminin (5 μg/mL), and within a few days neural rosettes began to appear. These rosettes were fed every second day with N2/B27 medium supplemented with the two SMAD inhibitors and laminin (1 μg/ml).

4.4. Generation of human cerebral organoids (COs)

Brain organoids were generated following the previously described protocol (Lancaster and Knoblich, 2014a). Briefly, hIPSCs grown in complete mTeSR1 were detached from the plates using Accutase® and resuspended in human embryonic stem cell (hESC) medium: DMEM/F12, 1 % Glutamax, 20 % of KnockOut™ Serum Replacement (KOSR), 3 % of hESC-quality fetal bovine serum (FBS), 0.1 mM of 2-mercaptoethanol (50 mM), 1 % of MEM-NEEA (100X) supplemented with bFGF (4 ng/mL) and the Rock inhibitor Y-27632 (5 μM, ROCKi). According to the established method, 9000 cells/well were seeded in round bottom ultra-low attachment 96-well plates. The next day, small EBs formed that were evident under a binocular stereomicroscope (Nikon) and these EBs were cultured for 5 days, refreshing the medium every two days, removing bFGF and ROCKi from day 4 onwards. After 6 days, the EBs were transferred to ultra-low attachment 24-well plates containing neural induction medium (NIM: DMEM/F12, 1 % Glutamax supplemented with 1 % N2™-supplement (100X), 1 % MEM-NEAA and 1 μg/mL heparin). The plates were maintained for a further 6 days, again changing the medium every two days. Once neuroectoderm differentiation was achieved (after approximately 5 days), neuroepithelium-induced EBs were embedded in Matrigel® to provide adequate three-dimensional support for the ensuing optimal development. The embedded EBs were collected in neural differentiation medium without vitamin A (NDM-vit A: 1:1 DMEM/F12-Neurobasal Medium, 1 % Glutamax, 0.5 % N2™-supplement (100X), 1 % B27 supplement (50X) without vitamin A, 0.5 % of MEM-NEEA solution (100X), 50 μM of 2-mercaptoethanol (50 mM), 1 % P/S (100X), 0.25 μg/mL antimycotic amphotericin B, and 2.5 μg/mL insulin) and transferred to a sterile P60 Petri dish. Embedded EBs were incubated for 4 days, changing the NDM-vit A medium every 48 h. Subsequently, the COs were transferred to an orbital shaker at 65 rpm to facilitate the flow of nutrients and oxygen, and the NDM + vit A medium was changed every 2–3 days. The COs were kept in culture for 30–60 days prior to further processing and throughout the CO generation procedure, the cells were kept at 37 °C in an atmosphere of 5 % CO_2 and ambient oxygen.

4.5. Reverse transcription and real-time quantitative PCR

At the time points indicated, total RNA was extracted from the hIPSCs, EBs or COs using the Speedtools total RNA extraction kit (Biotools), according to the manufacturer's instructions. To obtain enough RNA, 6 EBs or 3 COs were pooled and lysed by mechanical digestion in a homogenizer. In the case of COs, Matrigel® was previously removed by incubating with Dispase® (1 mg/mL) with agitation for 1 h at 37 °C. After digestion with TURBO DNase (Ambion), the total RNA was quantified in a Nanodrop One spectrophotometer (Thermo Fisher Scientific), and this RNA (1 μg) was reversed transcribed using M-MLV reverse transcriptase in the presence of random primers (6 μg) and dNTPs (350 μM: Invitrogen). Quantitative real-time PCR reactions (qPCR) were carried out using LuminoCt® qPCR Readymix (Sigma-Aldrich), 5 μL of the cDNA generated, gene-specific primers (Sigma Aldrich) and TaqMan MGB probes for human p2rx1, p2rx2, p2rx3, p2rx4, p2rx5, p2rx6, p2rx7 and gapdh (Roche). Fast thermal cycling was performed using a StepOnePlus™ Real-Time PCR System (Applied Biosystems) as follows: pre-denaturation at 95 °C for 20 s, followed by 40 cycles each of 95 °C for 1 s and 60 °C for 20 s. The results were normalized by parallel amplification with the control gapdh primers.

4.6. Immunoblotting

Total protein extracts were obtained from hIPSCs, 6–9 EBs or 6–9 COs lysed for 1 h at 4 °C in lysis buffer: 50 mM Tris/HCl, 150 mM NaCl, 1 % Nonidet P40 (pH 7.4), Complete™ Protease Inhibitor Cocktail tablets (Roche Diagnostics), 1 mM sodium orthovanadate (Sigma) and 1.5 μM okadaic acid (Calbiochem). Prior to lysis, the organoid Matrigel® was digested with Dispase® (1 mg/mL) for 1 h at 37 °C. The supernatants were harvested by centrifugation, quantified and equal amounts of protein extracts (20 μg) were resolved by 10 % Tris-Glycine SDS-PAGE. The protein was then transferred to nitrocellulose membranes (Amersham GE), which were blocked for 1h at room temperature (rt) with 5 % skimmed milk in PBS + 0.1 % Tween-20 (PBST) buffer, and they were probed overnight at 4 °C with primary antibodies against: P2X1 (1:200, 45 kDa), P2X2 (1:200, 45 kDa), P2X3 (1:200, 38 kDa), P2X4 (1:200, 42 kDa), P2X6 (1:200, 40 kDa), P2X7 (1:1.000, 70 kDa), or GAPDH (1:10.000, 36 kDa). The membranes were then washed three times with PBST and antibody binding was detected with a HRP-conjugated secondary goat anti-rabbit antibody (diluted 1:1.000). After 1 h, the membranes were washed three times with PBST and antibody binding was visualized by ECL using an HRP chemiluminescent substrate (PerkinElmer) on an ImageQuant LAS 500 Model (Amersham GE).

4.7. Immunohistofluorescence

At the time points indicated, COs were transferred individually to a 24-well plate containing PBS, fixed with 4 % PFA in PBS at rt for at least 2 h on an orbital shaker. After removing the PFA solution, the organoids were washed 3 times with PBS and then each CO was transferred to a 30 % sucrose solution in PBS and incubated for 48 h at 4 °C in a 2 mL Eppendorf tube. Subsequently, three pooled organoids were embedded in Tissue-Tek® OCT™ compound (Sakura), frozen on dry ice and stored

at −80 °C. Cryosections (20 μm) were then obtained on a CM1950 cryostat (Leica), mounted on ultrafrost slides, and incubated for 1 h at rt in blocking and permeabilization solution: 150 mM glycine, 4 % normal goat serum (NGS), and 0.25 % Triton X-100 (v/v) in PBS. The sections were probed overnight at 4 °C with primary antibodies diluted in blocking solution (150 mM glycine, 4 % NGS, 0.1 % Triton X-100 (v/v) in PBS) and subsequently, they were washed 3 times with PBS, and incubated with the secondary antibodies and with 1 μM DAPI at rt for 1 h. The slides were washed again 3 times with PBS and mounted in Aqua PolyMount medium (Polysciences).

The primary antibodies used in the immunohistofluorescence studies were: rabbit anti-P2X1 (1:50), rabbit anti-P2X4 (1:50), rabbit anti-P2X6 (1:50), mouse anti-nestin (1:200), rabbit anti-Sox2 (1:300), guinea pig anti-DCX (1:800), rabbit anti-Tbr2 (1:400), and rabbit anti-Ki67 (1:200). The secondary antibodies employed in the immunohistofluorescence assays were: donkey anti-guinea pig CyTM5 (1:500), goat anti-mouse Alexa Fluor™ 488 (1:500), and goat anti-rabbit Alexa Fluor™ 555 (1:500). The P2X1, P2X4, and P2X6 antibodies used required amplification of the fluorescence signal using goat anti-rabbit IgG Biotin (1:500) and Alexa Fluor™ 546 streptavidin (1:500). Fluorescence images were captured on a Leica TCS SPE confocal microscope (Leica Microsystems) controlled by the Leica LAS AF software, or a Leica SP8 confocal microscope with a LASX software (Leica Microsystems). Z-stack Images (20 μm thick and 1 μm Z-step) were acquired with an ApoPlan Fluor 40× oil immersion objective, and 405 nm, 488 nm, 552 nm and 647 nm laser lines. Leica SP8 images were obtained at the Unidad de Citometría de Flujo y Microscopía de Fluorescencia facility of the Complutense University of Madrid.

Confocal images of tissue sections were analyzed using the ImageJ software, initially processing the Z-stacks by creating a "Maximum Intensity" projection to combine slices. Subsequently, individual channels were separated, and specific regions of interest (ROIs) were defined based on the distribution of Nestin and DCX within the cortical regions. Masks were then generated for each channel according to the respective markers, and particles were counted within these defined regions using the 'Analyze Particles' function. A minimum size threshold of 10 nm was applied to ensure accurate particle detection. To analyze receptor distribution, the "Colocalization Threshold" option was used to compare the "RColoc" parameter across channels.

4.8. Microfluorimetric determination of intracellular free calcium concentrations

Neural rosettes cultured for 14 days on 15 mm diameter glass coverslips were washed with Locke's solution (140 mM NaCl, 4.7 mM KCl, 2.5 mM $CaCl_2$, 1.2 mM $MgSO_4$, 1.2 mM KH_2PO_4, 5.5 mM Glucose, 10 mM HEPES pH 7.4) and loaded with the Fura-2 AM calcium dye (7.5 μM) for 45 min at 37 °C. The coverslips were then washed with Locke's medium and placed in a superfusion chamber on the stage of a Nikon Eclipse TE-200 fluorescence microscope. The cells were continuously superfused with Locke's solution at 37 °C at a rate of approximately 1.5 ml/min. After registering the basal fluorescence in resting conditions, the cells were stimulated for 50 s with ATP at different concentrations (10 μM, 100 μM or 1 mM) to assess the presence of functional nucleotide receptors. The rosettes were visualized using a Plan Fluor 20X/0.5 lens and the wavelength of the incoming light (340 or 380 nm) was selected with an Optoscan monochromator with a 10 nm bandwidth (Cairn Research), acquiring 12-bit images with an ORCA-ER C 47 42–98 CCD camera (Hamamatsu) controlled by Metafluor 6.3r6 PC software (Universal Imaging Corp). The exposure time was 300 ms for each wavelength and the changing time was less than 5 msec. Fluorescence images were acquired continuously and buffered on a fast SCSI disk, the time course data representing the average light intensity in selected round regions within each neural rosette (at the center or periphery location). The background was subtracted at each wavelength and the ratio between the fluorescence registered after excitation at 340 and 380 nm was calculated. The data are represented as the fluorescence F_{340}/F_{380} ratio, which rises as the intracellular free calcium concentration increases.

4.9. Electrophysiology recordings

Electrophysiological recordings were obtained from neural rosettes grown for 14 days on 12 mm coverslips coated with poly L-ornithine (50 μg/mL) and laminin (5 μg/mL). The coverslips were submerged in a perfusion chamber with a continuous flow of extracellular solution: 145 mM NaCl, 2.8 mM KCl, 2 mM $CaCl_2$, 10 mM HEPES, 10 mM Glucose. Patch-clamp pipettes were made from borosilicate glass (ID/OD: 1.5/1.8 mm), pulled to a final resistance of ~5 MΩ, and filled with intracellular solution of the following composition:145 mM KCl, 8 mM NaCl, 10 mM HEPES, 0.3 mM EGTA, 1 mM $MgCl_2$, 2 mM ATP.Na_2, 0.3 mM GTP.Li_3.

The whole-cell voltage clamp configuration was used to record voltage or ligand-gated ionic currents. Holding voltage (V_h) was set to −80 mV, and the currents were filtered at 3 kHz and sampled at 10 kHz. Series resistance (<20 MΩ) was compensated by 80 % and monitored along with the capacitance of the cell membrane throughout the experiment. Voltage-dependent currents were induced by 100 msec depolarizations to +10 mV, and ligand-gated currents were elicited by (ATP 1 mM, 3 s). ATP dissolved in extracellular solution was applied directly to the cell under investigation through a pneumatic pressure drug ejection system (PDES-02DX, NPI Electronic GmbH, Germany), using a borosilicate pipette with a 3–5 μm opening placed near the cell (5–10 μm). Membrane potential changes were evoked by depolarizing current injection and measured in the current-clamp mode of the whole-cell configuration from a of voltage (V_{comm}) of −70 mV.

4.10. Data processing and analysis

GraphPad Prism 10 software was employed for the statistical analysis of the results. Comparisons were performed using one-way analysis of variance (ANOVA) with Dunnett's post-test to compare different conditions against the control group. When only two groups were compared, an unpaired *t*-test with Welch's correction was used to account for unequal variances. Significance was defined as: ****P < 0.0001, ***P < 0.001, **P < 0.01, *P < 0.05. P values greater than 0.05 were considered non-significant (NS).

CRediT authorship contribution statement

María Benito-León: Methodology, Formal analysis, Data curation. **Julia Serrano-López:** Methodology, Formal analysis, Data curation. **Celia Llorente-Sáez:** Methodology, Formal analysis, Data curation. **Marina Arribas-Blázquez:** Writing – original draft, Methodology, Formal analysis, Data curation. **Luis A. Olivos-Oré:** Writing – original draft, Methodology, Formal analysis, Data curation. **Veronica Pravata:** Formal analysis, Data curation. **Raquel Pérez-Sen:** Writing – original draft, Validation, Methodology, Formal analysis, Data curation. **Esmerilda G. Delicado:** Writing – original draft, Visualization, Validation, Formal analysis, Data curation. **Micha Drukker:** Visualization, Validation, Resources, Methodology. **Antonio R. Artalejo:** Writing – original draft, Visualization, Validation, Methodology, Formal analysis, Data curation. **Silvia Cappello:** Visualization, Validation, Resources, Methodology, Formal analysis, Data curation. **Rosa Gómez-Villafuertes:** Writing – original draft, Supervision, Methodology, Formal analysis, Data curation, Conceptualization. **Felipe Ortega:** Writing – review & editing, Writing – original draft, Supervision, Methodology, Investigation, Funding acquisition, Formal analysis, Conceptualization.

Declaration of competing interest

The authors declare that they have no known competing financial

interests or personal relationships that could have appeared to influence the work reported in this paper.

Acknowledgments

This work was supported by grants from the Ministerio de Ciencia, Innovación y Universidades (MICIU, PID2022-138073OB-I00), the Red de Excelencia Consolider-Ingenio Spanish Ion Channel Initiative (BFU2015-70067REDC) and the Fundación Ramón Areces (PR2018/16-02). The work described in this article was also supported by the COST Action CA21130 "P2X receptors as a therapeutic opportunity (PRESTO)". MB-L was supported by "Fondo de Garantía Juvenil, Comunidad de Madrid" CAM PEJD-2016/BMD-2572. J.S.L. was supported by UCM-Santander grants program (PR26/16-18B-3).

Appendix A. Supplementary data

Supplementary data to this article can be found online at https://doi.org/10.1016/j.neuropharm.2025.110784.

References

Abbracchio, M.P., Burnstock, G., Verkhratsky, A., Zimmermann, H., 2009. Purinergic signalling in the nervous system: an overview. Trends Neurosci. 32, 19–29.
Bankston, L.A., Guidotti, G., 1996. Characterization of ATP transport into chromaffin granule ghosts. Synergy of ATP and serotonin accumulation in chromaffin granule ghosts. J. Biol. Chem. 271, 17132–17138.
Battal, B., Ince, S., Akgun, V., Kocaoglu, M., Ozcan, E., Tasar, M., 2015. Malformations of cortical development: 3T magnetic resonance imaging features. World J. Radiol. 7, 329–335.
Berg, D.A., Belnoue, L., Song, H., Simon, A., 2013. Neurotransmitter-mediated control of neurogenesis in the adult vertebrate brain. Development 140, 2548–2561.
Bestman, J.E., Stackley, K.D., Rahn, J.J., Williamson, T.J., Chan, S.S., 2015. The cellular and molecular progression of mitochondrial dysfunction induced by 2,4-dinitrophenol in developing zebrafish embryos. Differentiation 89, 51–69.
Bhaduri, A., Andrews, M.G., Mancia Leon, W., Jung, D., Shin, D., Allen, D., Jung, D., Schmunk, G., Haeussler, M., Salma, J., et al., 2020. Cell stress in cortical organoids impairs molecular subtype specification. Nature 578, 142–148.
Budday, S., Steinmann, P., Kuhl, E., 2015. Physical biology of human brain development. Front. Cell. Neurosci. 9, 257.
Burnstock, G., 1972. Purinergic nerves. Pharmacol. Rev. 24, 509–581.
Burnstock, G., 2007a. Physiology and pathophysiology of purinergic neurotransmission. Physiol. Rev. 87, 659–797.
Burnstock, G., 2007b. Purine and pyrimidine receptors. Cell. Mol. Life Sci. 64, 1471–1483.
Burnstock, G., Campbell, G., Satchell, D., Smythe, A., 1970. Evidence that adenosine triphosphate or a related nucleotide is the transmitter substance released by non-adrenergic inhibitory nerves in the gut. Br. J. Pharmacol. 40, 668–688.
Burnstock, G., Fredholm, B.B., Verkhratsky, A., 2011. Adenosine and ATP receptors in the brain. Curr. Top. Med. Chem. 11, 973–1011.
Cakir, B., Xiang, Y., Tanaka, Y., Kural, M.H., Parent, M., Kang, Y.J., Chapeton, K., Patterson, B., Yuan, Y., He, C.S., et al., 2019. Engineering of human brain organoids with a functional vascular-like system. Nat. Methods 16, 1169–1175.
Cardenas, A., Villalba, A., de Juan Romero, C., Pico, E., Kyrousi, C., Tzika, A.C., Tessier-Lavigne, M., Ma, L., Drukker, M., Cappello, S., et al., 2018. Evolution of cortical neurogenesis in amniotes controlled by robo signaling levels. Cell 174, 590–606 e521.
Cheung, K.K., Burnstock, G., 2002. Localization of P2X3 receptors and coexpression with P2X2 receptors during rat embryonic neurogenesis. J. Comp. Neurol. 443, 368–382.
Cheung, K.K., Ryten, M., Burnstock, G., 2003. Abundant and dynamic expression of G protein-coupled P2Y receptors in mammalian development. Dev. Dyn. 228, 254–266.
Conti, L., Cattaneo, E., 2010. Neural stem cell systems: physiological players or in vitro entities? Nat. Rev. Neurosci. 11, 176–187.
del Puerto, A., Diaz-Hernandez, J.I., Tapia, M., Gomez-Villafuertes, R., Benitez, M.J., Zhang, J., Miras-Portugal, M.T., Wandosell, F., Diaz-Hernandez, M., Garrido, J.J., 2012. Adenylate cyclase 5 coordinates the action of ADP, P2Y1, P2Y13 and ATP-gated P2X7 receptors on axonal elongation. J. Cell Sci. 125, 176–188.
Diaz-Hernandez, J.I., Gomez-Villafuertes, R., Leon-Otegui, M., Hontecillas-Prieto, L., Del Puerto, A., Trejo, J.L., Lucas, J.J., Garrido, J.J., Gualix, J., Miras-Portugal, M.T., et al., 2012. In vivo P2X7 inhibition reduces amyloid plaques in Alzheimer's disease through GSK3beta and secretases. Neurobiol. Aging 33, 1816–1828.
Diaz-Hernandez, M., del Puerto, A., Diaz-Hernandez, J.I., Diez-Zaera, M., Lucas, J.J., Garrido, J.J., Miras-Portugal, M.T., 2008. Inhibition of the ATP-gated P2X7 receptor promotes axonal growth and branching in cultured hippocampal neurons. J. Cell Sci. 121, 3717–3728.
Egan, T.M., Samways, D.S.K., Li, Z., 2006. Biophysics of P2X receptors. Pflügers Archiv 452, 501–512.
Engel, T., Gomez-Villafuertes, R., Tanaka, K., Mesuret, G., Sanz-Rodriguez, A., Garcia-Huerta, P., Miras-Portugal, M.T., Henshall, D.C., Diaz-Hernandez, M., 2012. Seizure suppression and neuroprotection by targeting the purinergic P2X7 receptor during status epilepticus in mice. FASEB J. 26, 1616–1628.
Fietz, S.A., Kelava, I., Vogt, J., Wilsch-Brauninger, M., Stenzel, D., Fish, J.L., Corbeil, D., Riehn, A., Distler, W., Nitsch, R., et al., 2010. OSVZ progenitors of human and ferret neocortex are epithelial-like and expand by integrin signaling. Nat. Neurosci. 13, 690–699.
Fumagalli, M., Lecca, D., Abbracchio, M.P., Ceruti, S., 2017. Pathophysiological role of purines and pyrimidines in neurodevelopment: unveiling new pharmacological approaches to congenital brain diseases. Front. Pharmacol. 8, 941.
Furutachi, S., Miya, H., Watanabe, T., Kawai, H., Yamasaki, N., Harada, Y., Imayoshi, I., Nelson, M., Nakayama, K.I., Hirabayashi, Y., et al., 2015. Slowly dividing neural progenitors are an embryonic origin of adult neural stem cells. Nat. Neurosci. 18, 657–665.
Giachino, C., Barz, M., Tchorz, J.S., Tome, M., Gassmann, M., Bischofberger, J., Bettler, B., Taylor, V., 2014. GABA suppresses neurogenesis in the adult hippocampus through GABAB receptors. Development 141, 83–90.
Glaser, T., de Oliveira, S.L., Cheffer, A., Beco, R., Martins, P., Fornazari, M., Lameu, C., Junior, H.M., Coutinho-Silva, R., Ulrich, H., 2014. Modulation of mouse embryonic stem cell proliferation and neural differentiation by the P2X7 receptor. PLoS One 9, e96281.
Glaser, T., Resende, R.R., Ulrich, H., 2013. Implications of purinergic receptor-mediated intracellular calcium transients in neural differentiation. Cell Commun. Signal. 11, 12.
Gomez-Villafuertes, R., del Puerto, A., Diaz-Hernandez, M., Bustillo, D., Diaz-Hernandez, J.I., Huerta, P.G., Artalejo, A.R., Garrido, J.J., Miras-Portugal, M.T., 2009. Ca2+/calmodulin-dependent kinase II signalling cascade mediates P2X7 receptor-dependent inhibition of neuritogenesis in neuroblastoma cells. FEBS J. 276, 5307–5325.
Gualix, J., Abal, M., Pintor, J., Garcia-Carmona, F., Miras-Portugal, M.T., 1996. Nucleotide vesicular transporter of bovine chromaffin granules. Evidence for a mnemonic regulation. J. Biol. Chem. 271, 1957–1965.
Gualix, J., Alvarez, A.M., Pintor, J., Miras-Portugal, M.T., 1999. Studies of chromaffin granule functioning by flow cytometry: transport of fluorescent epsilon-ATP and granular size increase induced by ATP. Recept. Channel 6, 449–461.
Guerrini, R., Dobyns, W.B., 2014. Malformations of cortical development: clinical features and genetic causes. Lancet Neurol. 13, 710–726.
Guo, W., Zhang, Z., Liu, X., Burnstock, G., Xiang, Z., He, C., 2013. Developmental expression of P2X5 receptors in the mouse prenatal central and peripheral nervous systems. Purinergic Signal. 9, 239–248.
Hansen, D.V., Lui, J.H., Parker, P.R., Kriegstein, A.R., 2010. Neurogenic radial glia in the outer subventricular zone of human neocortex. Nature 464, 554–561.
He, Z., Dony, L., Fleck, J.S., Szalata, A., Li, K.X., Sliskovic, I., Lin, H.C., Santel, M., Atamian, A., Quadrato, G., et al., 2024. An integrated transcriptomic cell atlas of human neural organoids. Nature 635, 690–698.
Illes, P., Muller, C.E., Jacobson, K.A., Grutter, T., Nicke, A., Fountain, S.J., Kennedy, C., Schmalzing, G., Jarvis, M.F., Stojilkovic, S.S., et al., 2021. Update of P2X receptor properties and their pharmacology: IUPHAR Review 30. Br. J. Pharmacol. 178, 489–514.
Kanton, S., Boyle, M.J., He, Z., Santel, M., Weigert, A., Sanchis-Calleja, F., Guijarro, P., Sidow, L., Fleck, J.S., Han, D., et al., 2019. Organoid single-cell genomic atlas uncovers human-specific features of brain development. Nature 574, 418–422.
Kriegstein, A., Alvarez-Buylla, A., 2009. The glial nature of embryonic and adult neural stem cells. Annu. Rev. Neurosci. 32, 149–184.
Kyrousi, C., Cappello, S., 2020. Using brain organoids to study human neurodevelopment, evolution and disease. Wiley Interdiscip. Rev. Dev. Biol. 9, e347.
Lancaster, M.A., Knoblich, J.A., 2014a. Generation of cerebral organoids from human pluripotent stem cells. Nat. Protoc. 9, 2329–2340.
Lancaster, M.A., Knoblich, J.A., 2014b. Organogenesis in a dish: modeling development and disease using organoid technologies. Science 345, 1247125.
Lancaster, M.A., Renner, M., Martin, C.A., Wenzel, D., Bicknell, L.S., Hurles, M.E., Homfray, T., Penninger, J.M., Jackson, A.P., Knoblich, J.A., 2013. Cerebral organoids model human brain development and microcephaly. Nature 501, 373–379.
Leon-Otegui, M., Gomez-Villafuertes, R., Diaz-Hernandez, J.I., Diaz-Hernandez, M., Miras-Portugal, M.T., Gualix, J., 2011. Opposite effects of P2X7 and P2Y2 nucleotide receptors on alpha-secretase-dependent APP processing in Neuro-2a cells. FEBS Lett. 585, 2255–2262.
Lucía Paniagua-Herranz, J.S.-L., Llorente-Sáez, Celia, Pérez-Sanz, Marina Leonor, Agustín-Durán, David de, Duart-Abadia, Pere, Domingo-Muelas, Ana, Vincelle-Nieto, África, Bragado, Paloma, Manzano-Franco, Diana, Arribas-Blázquez, Marina, Alcides Olivos-Oré, Luis, Gascón, Sergio, Gutierrez-Uzquiza, Álvaro, Pérez-Sen, Raquel, Delicado, Esmerilda G., Gómez-Villafuertes, Rosa, Reyes-Palomares, Armando, Artalejo, Antonio R., Fariñas, Isabel, Ortega, Felipe, 2024. Purinergic receptor P2Y13 controls activation and mode of division in subependymal adult neural stem cells. bioRxiv.
Menendez-Mendez, A., Diaz-Hernandez, J.I., Miras-Portugal, M.T., 2015. The vesicular nucleotide transporter (VNUT) is involved in the extracellular ATP effect on neuronal differentiation. Purinergic Signal. 11, 239–249.
Menendez-Mendez, A., Diaz-Hernandez, J.I., Ortega, F., Gualix, J., Gomez-Villafuertes, R., Miras-Portugal, M.T., 2017. Specific temporal distribution and subcellular localization of a functional vesicular nucleotide transporter (VNUT) in cerebellar granule neurons. Front. Pharmacol. 8, 951.
Miras-Portugal, M.T., Diaz-Hernandez, J.I., Gomez-Villafuertes, R., Diaz-Hernandez, M., Artalejo, A.R., Gualix, J., 2015. Role of P2X7 and P2Y2 receptors on alpha-secretase-

dependent APP processing: control of amyloid plaques formation "in vivo" by P2X7 receptor. Comput. Struct. Biotechnol. J. 13, 176–181.
Miras-Portugal, M.T., Gomez-Villafuertes, R., Gualix, J., Diaz-Hernandez, J.I., Artalejo, A.R., Ortega, F., Delicado, E.G., Perez-Sen, R., 2016. Nucleotides in neuroregeneration and neuroprotection. Neuropharmacology 104, 243–254.
Miras-Portugal, M.T., Menendez-Mendez, A., Gomez-Villafuertes, R., Ortega, F., Delicado, E.G., Perez-Sen, R., Gualix, J., 2019. Physiopathological role of the vesicular nucleotide transporter (VNUT) in the central nervous System: relevance of the vesicular nucleotide release as a potential therapeutic target. Front. Cell. Neurosci. 13, 224.
Miras-Portugal, M.T., Sebastian-Serrano, A., de Diego Garcia, L., Diaz-Hernandez, M., 2017. Neuronal P2X7 receptor: involvement in neuronal physiology and pathology. J. Neurosci. 37, 7063–7072.
Molnar, Z., Clowry, G.J., Sestan, N., Alzu'bi, A., Bakken, T., Hevner, R.F., Huppi, P.S., Kostovic, I., Rakic, P., Anton, E.S., et al., 2019. New insights into the development of the human cerebral cortex. J. Anat. 235, 432–451.
Noctor, S.C., Flint, A.C., Weissman, T.A., Wong, W.S., Clinton, B.K., Kriegstein, A.R., 2002. Dividing precursor cells of the embryonic cortical ventricular zone have morphological and molecular characteristics of radial glia. J. Neurosci. 22, 3161–3173.
O'Neill, A.C., Kyrousi, C., Einsiedler, M., Burtscher, I., Drukker, M., Markie, D.M., Kirk, E.P., Gotz, M., Robertson, S.P., Cappello, S., 2018. Mob2 Insufficiency disrupts neuronal migration in the developing cortex. Front. Cell. Neurosci. 12, 57.
Okita, K., Matsumura, Y., Sato, Y., Okada, A., Morizane, A., Okamoto, S., Hong, H., Nakagawa, M., Tanabe, K., Tezuka, K., et al., 2011. A more efficient method to generate integration-free human iPS cells. Nat. Methods 8, 409–412.
Oliveira, A., Illes, P., Ulrich, H., 2016. Purinergic receptors in embryonic and adult neurogenesis. Neuropharmacology 104, 272–281.
Oliveira, S.L., Trujillo, C.A., Negraes, P.D., Ulrich, H., 2015. Effects of ATP and NGF on proliferation and migration of neural precursor cells. Neurochem. Res. 40, 1849–1857.
Ortega, F., Gomez-Villafuertes, R., Benito-Leon, M., Martinez de la Torre, M., Olivos-Ore, L.A., Arribas-Blazquez, M., Gomez-Gaviro, M.V., Azcorra, A., Desco, M., Artalejo, A.R., et al., 2021. Salient brain entities labelled in P2rx7-EGFP reporter mouse embryos include the septum, roof plate glial specializations and circumventricular ependymal organs. Brain Struct. Funct. 226, 715–741.
Ortega, F., Perez-Sen, R., Delicado, E.G., Miras-Portugal, M.T., 2009. P2X7 nucleotide receptor is coupled to GSK-3 inhibition and neuroprotection in cerebellar granule neurons. Neurotox. Res. 15, 193–204.
Ortega, F., Perez-Sen, R., Delicado, E.G., Teresa Miras-Portugal, M., 2011. ERK1/2 activation is involved in the neuroprotective action of P2Y13 and P2X7 receptors against glutamate excitotoxicity in cerebellar granule neurons. Neuropharmacology 61, 1210–1221.
Ortega, F., Perez-Sen, R., Morente, V., Delicado, E.G., Miras-Portugal, M.T., 2010. P2X7, NMDA and BDNF receptors converge on GSK3 phosphorylation and cooperate to promote survival in cerebellar granule neurons. Cell. Mol. Life Sci. 67, 1723–1733.
Paniagua-Herranz, L., Menendez-Mendez, A., Gomez-Villafuertes, R., Olivos-Ore, L.A., Biscaia, M., Gualix, J., Perez-Sen, R., Delicado, E.G., Artalejo, A.R., Miras-Portugal, M.T., et al., 2020. Live imaging reveals cerebellar neural stem cell dynamics and the role of VNUT in lineage progression. Stem Cell Rep. 15, 1080–1094.
Park, D.S., Kozaki, T., Tiwari, S.K., Moreira, M., Khalilnezhad, A., Torta, F., Olivie, N., Thiam, C.H., Liani, O., Silvin, A., et al., 2023. iPS-cell-derived microglia promote brain organoid maturation via cholesterol transfer. Nature 623, 397–405.
Pellegrini, L., Bonfio, C., Chadwick, J., Begum, F., Skehel, M., Lancaster, M.A., 2020. Human CNS barrier-forming organoids with cerebrospinal fluid production. Science 369.
Queipo, M.J., Gil-Redondo, J.C., Morente, V., Ortega, F., Miras-Portugal, M.T., Delicado, E.G., Perez-Sen, R., 2017. P2X7 nucleotide and EGF receptors exert dual modulation of the dual-specificity phosphatase 6 (MKP-3) in granule neurons and astrocytes, contributing to negative feedback on ERK signaling. Front. Mol. Neurosci. 10, 448.
Renner, M., Lancaster, M.A., Bian, S., Choi, H., Ku, T., Peer, A., Chung, K., Knoblich, J.A., 2017. Self-organized developmental patterning and differentiation in cerebral organoids. EMBO J. 36, 1316–1329.
Resende, R.R., Britto, L.R., Ulrich, H., 2008. Pharmacological properties of purinergic receptors and their effects on proliferation and induction of neuronal differentiation of P19 embryonal carcinoma cells. Int. J. Dev. Neurosci. 26, 763–777.
Sawada, K., Echigo, N., Juge, N., Miyaji, T., Otsuka, M., Omote, H., Yamamoto, A., Moriyama, Y., 2008. Identification of a vesicular nucleotide transporter. Proc. Natl. Acad. Sci. U. S. A. 105, 5683–5686.
Schwindt, T.T., Trujillo, C.A., Negraes, P.D., Lameu, C., Ulrich, H., 2011. Directed differentiation of neural progenitors into neurons is accompanied by altered expression of P2X purinergic receptors. J. Mol. Neurosci. 44, 141–146.
Smart, I.H., Dehay, C., Giroud, P., Berland, M., Kennedy, H., 2002. Unique morphological features of the proliferative zones and postmitotic compartments of the neural epithelium giving rise to striate and extrastriate cortex in the monkey. Cerebr. Cortex 12, 37–53.
Song, J., Zhong, C., Bonaguidi, M.A., Sun, G.J., Hsu, D., Gu, Y., Meletis, K., Huang, Z.J., Ge, S., Enikolopov, G., et al., 2012. Neuronal circuitry mechanism regulating adult quiescent neural stem-cell fate decision. Nature 489, 150–154.
Suzuki, M., Nelson, A.D., Eickstaedt, J.B., Wallace, K., Wright, L.S., Svendsen, C.N., 2006. Glutamate enhances proliferation and neurogenesis in human neural progenitor cell cultures derived from the fetal cortex. Eur. J. Neurosci. 24, 645–653.
Tang, Y., Illes, P., 2017. Regulation of adult neural progenitor cell functions by purinergic signaling. Glia 65, 213–230.
Tong, C.K., Chen, J., Cebrian-Silla, A., Mirzadeh, Z., Obernier, K., Guinto, C.D., Tecott, L. H., Garcia-Verdugo, J.M., Kriegstein, A., Alvarez-Buylla, A., 2014. Axonal control of the adult neural stem cell niche. Cell Stem Cell 14, 500–511.
Topol, A., Tran, N.N., Brennand, K.J., 2015. A guide to generating and using hiPSC derived NPCs for the study of neurological diseases. J. Vis. Exp., e52495
Trinchero, M.F., Giacomini, D., Schinder, A.F., 2021. Dynamic interplay between GABAergic networks and developing neurons in the adult hippocampus. Curr. Opin. Neurobiol. 69, 124–130.
Velasco, S., Kedaigle, A.J., Simmons, S.K., Nash, A., Rocha, M., Quadrato, G., Paulsen, B., Nguyen, L., Adiconis, X., Regev, A., et al., 2019. Individual brain organoids reproducibly form cell diversity of the human cerebral cortex. Nature 570, 523–527.
Villalba, A., Gotz, M., Borrell, V., 2021. The regulation of cortical neurogenesis. Curr. Top. Dev. Biol. 142, 1–66.
von Kugelgen, I., Hoffmann, K., 2016. Pharmacology and structure of P2Y receptors. Neuropharmacology 104, 50–61.
Weissman, T.A., Riquelme, P.A., Ivic, L., Flint, A.C., Kriegstein, A.R., 2004. Calcium waves propagate through radial glial cells and modulate proliferation in the developing neocortex. Neuron 43, 647–661.
Xiang, Y., Tanaka, Y., Patterson, B., Kang, Y.J., Govindaiah, G., Roselaar, N., Cakir, B., Kim, K.Y., Lombroso, A.P., Hwang, S.M., et al., 2017. Fusion of regionally specified hPSC-Derived organoids models human brain development and interneuron migration. Cell Stem Cell 21, 383–398 e387.
Xing, L., Huttner, W.B., 2020. Neurotransmitters as modulators of neural progenitor cell proliferation during mammalian neocortex development. Front. Cell Dev. Biol. 8, 391.
Young, A., Machacek, D.W., Dhara, S.K., Macleish, P.R., Benveniste, M., Dodla, M.C., Sturkie, C.D., Stice, S.L., 2011. Ion channels and ionotropic receptors in human embryonic stem cell derived neural progenitors. Neuroscience 192, 793–805.
Zhang, W., Jiang, J., Xu, Z., Yan, H., Tang, B., Liu, C., Chen, C., Meng, Q., 2023. Microglia-containing human brain organoids for the study of brain development and pathology. Mol. Psychiatr. 28, 96–107.
Zimmermann, H., 2006. Nucleotide signaling in nervous system development. Pflügers Archiv 452, 573–588.
Zimmermann, H., 2021. History of ectonucleotidases and their role in purinergic signaling. Biochem. Pharmacol. 187, 114322.